Hydroclimatic changes in the British Isles through the Last-Glacial-Interglacial Transition: multiproxy reconstructions from the Vale of Pickering, NE England.

Lincoln, P.C. [a, b], Matthews, I.P. [a], Palmer, A.P. [a], Blockley, S.P.E. [a], Staff, R.A. [c], Candy, I. [a]

[a] Centre for Quaternary Research, Department of Geography, Royal Holloway, University of London, Egham, UK.

[b] Present address: School of Archaeology, Geography and Environmental Science, University of Reading, Earley, UK

[c] Scottish Universities Environmental Research Centre, University of Glasgow, East Kilbride, UK

Abstract

European paleoenvironmental records through the Last Glacial-Interglacial Transition (LGIT; *ca* 16-11 cal ka BP) record a series of climatic events occurring over decadal to multi-centennial timescales. Changes in components of the climatic system other than temperature (e.g. hydrology) through the LGIT are relatively poorly understood however, and further records of hydroclimatic changes are required in order to develop a more complete understanding of the phasing of environmental and anthropogenic responses in Europe to abrupt climate change. Here, we present a high-resolution, multiproxy palaeoenvironmental record (macroscale & microscale sedimentology, macrofossils, & bulk carbonate stable isotopes), from a palaeolake sequence in the Vale of Pickering (VoP), NE England, which enables the reconstruction of hydroclimatic changes constrained by a radiocarbon-based chronology. Relative lake-level changes in the VoP occurred in close association (although not necessarily in phase) to threshold shifts across abrupt climate change transitions, most notably lowering during cooling intervals of the LGIT (~GI-1d, ~GI-1b, and ~GS-1). This reflects more arid hydroclimates associated with these cooling episodes in the British Isles. Comparisons to hydrological records elsewhere in Europe show a latitudinal bifurcation, with Northern Europe (50-60°N) becoming more arid (humid), and Southern Europe (40-50°N) becoming more humid (arid) in response to these cooling (warming) intervals. We attribute these bifurcating signals to the relative positions of the Atlantic storm tracks, sea-ice margin, and North Atlantic Polar Front (NAPF) during the climatic events of the LGIT.

1. Introduction

The Last Glacial-Interglacial Transition (LGIT; *ca* 16-11 cal ka BP) is the most recent period where the climate system underwent large-scale reorganisation of ocean and atmospheric circulation (Heiri *et al.,* 2014; Rahmstorf *et al.,* 2015). The stratotype for the LGIT in the circum-North Atlantic region is the Greenland $\delta^{18}O$ event stratigraphy, where a series of abrupt and short-lived (millennial to sub-centennial scale) climatic events (GI-1d, GI-1c2, GI-1b, GS-1, 11.4 ka event), are superimposed upon a millennial-scale warming trend (Rasmussen *et al.,* 2014). These climatic events have end members of near interglacial to almost full glacial conditions (Rasmussen *et al.,* 2006; Lowe *et al.,* 2008) and transition between these at sub-decadal timescales (Steffensen *et al.,* 2008). Their causes are debated, but they most likely derive from fluctuations in the strength and position of the Atlantic Meridional Overturning Circulation (AMOC) in the North Atlantic Ocean, driven by freshwater forcing from the deglaciation of Northern Hemispheric ice sheets (Broecker and Denton, 1989; Clark et al., 2002; Marshall et al., 2007). These processes are projected to play an important role in future climatic change and therefore the LGIT provides a crucial interval in which to improve understanding on the terrestrial and hydrological responses to intervals of abrupt climatic change in Europe (e.g. Vellinga and Wood, 2002; Heiri et al., 2014).

The pattern of climatic change is well established in Greenland, but climatic signals across the mid-latitudes of the North Atlantic seaboard are less well understood. Whilst it is accepted that they show a similar pattern to those in the Greenland ice-core records at millennial time scales, spatial differences in magnitude and the synchronicity of the shorter-lived climatic oscillations and transitions remain largely untested assumptions (e.g. Lowe et al., 1995). There has been a specific focus on proxies of past temperature (e.g. Atkinson *et al.,* 1987; Yu and Eicher, 1998; von Grafenstein et al., 1999; Brooks and Birks, 2000; Marshall et al., 2002; Brooks et al., 2012) with few studies focused on, or able to identify, variations in other aspects of the climatic system such as hydrological changes, which would have also had a substantial impact on glacier ice growth and decay (e.g. Boston et al., 2015; Mangerud et al., 2016; Chandler et al., 2019; Lowe et al., 2019), fluvial activity (e.g. Vandenberghe, 2008), vegetation cover (e.g. Birks and Birks, 2014) and phases of human migration and subsistence (e.g. Blockley et al., 2018) in Europe. This realisation has led to a renewed interest in studies which provide data encompassing both temperature and past hydrological variations (e.g. Renssen et al., 2018). A limited number of key high resolution records of climatic and environmental responses for this period suggest three key aspects: (1) the transitions in to- and out of- the major intervals of the LGIT (i.e. the start of GI-1, GS-1, the Holocene) were regionally diachronous (Buizert et al., 2014; Rach et al., 2014; Muschitiello et al., 2015); (2) there are centennial-scale climatic events in Europe that have no correlative in the Greenland ice-core $\delta^{18}O$ stratigraphy (e.g.

Bakke et al., 2009; Lane et al., 2013; Guillevic et al., 2016; Blockley et al. 2018); and (3) the hydroclimatic impact of these climatic events across Europe was heterogeneous (e.g. Magny et al., 2003; Moreno et al., 2014; Renssen et al., 2018). These studies highlight the need for additional high-resolution records of past hydroclimates to test whether during the abrupt climatic transitions of the LGIT, hydroclimatic responses across the North Atlantic seaboard were spatially complex, not synchronised, different in expression, and that the Greenland $\delta^{18}O$ profiles cannot be used as a single comparative record (e.g. Guillevic et al., 2014; Muschitiello et al., 2015; Landais et al., 2018).

This paper presents a new, high-resolution, multiproxy palaeo-record from the Vale of Pickering (VoP) in NE England (54.2 ºN, 0.7 ºW; Figure 1) with the aims of:

- Reconstructing temperature and hydrological changes (carbonate $\delta^{18}O$ and relative lake-level) through the LGIT.
- Placing the hydroclimatic changes upon a calendar timescale, with precision comparable to the Greenland ice cores using a Bayesian-based radiocarbon age model.
- Comparing the regional hydroclimatic changes across Europe and Greenland through the LGIT.

2. Site context

The VoP is a low-lying valley in NE England situated adjacent to the North Sea coast (Figure 1). Between *ca* 25 and 17 ka BP, the North Sea Ice Lobe (NSIL) advanced and retreated into the eastern 12 km of the VoP, depositing a complex series of glacial, glaciolacustrine (Kendall, 1902; Evans et al., 2017), and glaciofluvial deposits (Palmer et al., 2015; Lincoln et al., 2017). Palaeobasins were formed within topographic depressions in these sediments after ice recession, which were subsequently infilled with lacustrine and alluvial sediments through the LGIT (Lincoln et al., 2017). The largest of these palaeobasins, Palaeolake Flixton (*ca* 4.2 km^2) has been extensively investigated via sedimentological (Palmer et al., 2015), palaeoenvironmental (Day, 1996; Candy et al., 2015; Blockley et al., 2018) and archaeological (Mellars and Dark, 1998; Milner et al., 2018) surveys. These studies have shown that palaeolake records in the eastern VoP have significant potential to reconstruct palaeoenvironmental regimes, but that the sediments from Palaeolake Flixton contain limited terrestrial plant macrofossil remains required for the generation of robust, radiocarbon-based age models prior to the Holocene (Day, 1996; Blockley et al., 2018). Furthermore, the sedimentary sequences contained within Palaeolake Flixton suggest substantial changes in lake-level that have been tentatively linked to broader hydrological shifts (Palmer *et al.,* 2015).

However, these shifts have yet to be independently corroborated, meaning their link to the hydrology of the eastern VoP, and regional climatic changes remain unresolved.

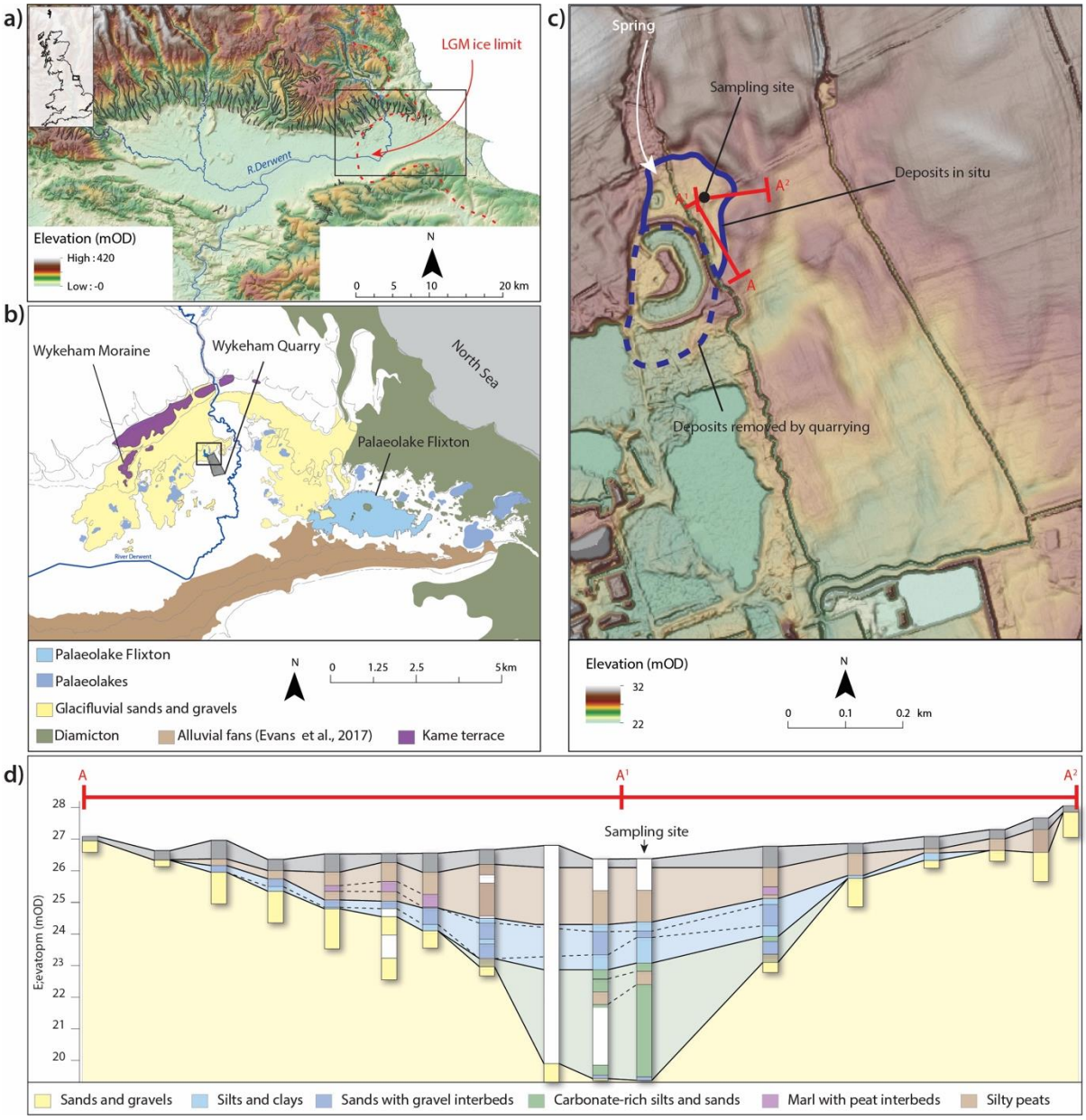

Figure 1. a) Digital Elevation Model (DEM) of the VoP with the LGM ice limit marked in red; b) map from Lincoln et al. (2017) showing the distribution of glacigenic sediments and palaeobasins in the eastern VoP (outlined in in black a)), the location of Wykeham Quarry is marked in grey; c) LiDAR DEM of the study site, showing the extent of the palaeobasin and the sampling location of the sedimentary sequence; d) cross-section of the palaeolake, illustrating that the sedimentology and stratigraphy of the sampled sequence is representative of the broader palaeolake deposits.

Consequently, other palaeolakes in the eastern VoP were sought in the vicinity of Palaeolake Flixton, using desk-based GIS and depositional modelling around the Wykeham Quarry area. A new kettlehole palaeolake, referred to as the Wykeham basin, was identified in glacifluvial outwash deposits ~ 4km east of Palaeolake Flixton (Lincoln et al., 2017). The deposits in the Wykeham basin are potentially better suited to reconstruct and constrain hydroclimatic changes in the valley as it is a smaller (*ca* 0.03 km^2) and simpler palaeolake system than Palaeolake Flixton (Figure 1b).

3. Methodology

3.1. Sediment recovery and analysis

The extent, thickness, and sedimentology of the Wykeham basin infill was evaluated by exploratory augering with Eijkelkamp open gouge percussion coring, Russian coring, and deposit modelling of the area around Wykeham Quarry (Lincoln et al., 2017). This showed that the southwestern extent of the basin had been removed by quarrying, but the northern and eastern sections remain *in situ* (Figure 1; Batchelor, 2009; Lincoln et al., 2017). A further twenty-two overlapping hand augered Russian- and percussion augered stitz cores were obtained from five parallel boreholes spaced < 5 m apart in the deepest section of the basin (SE 98656 83093). A composite 6.80 m stratigraphy was constructed by correlating overlapping cores using key marker horizons and patterns in bulk sedimentology (Figure 2).

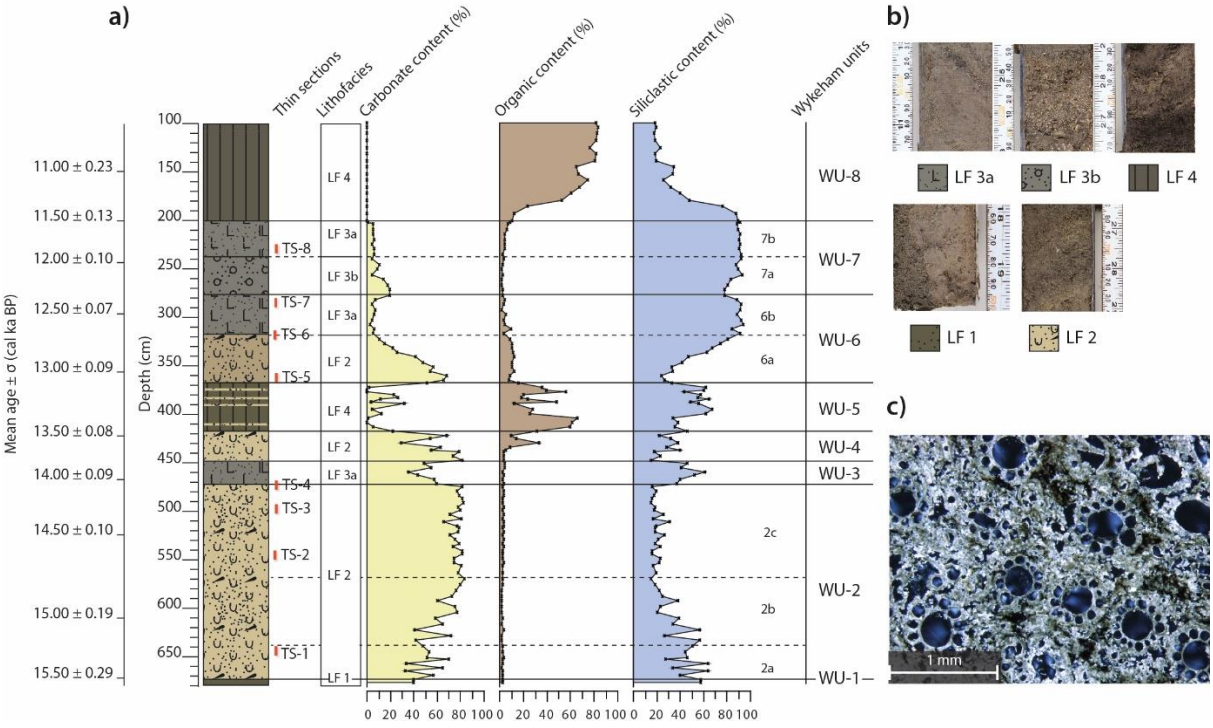

Figure 2. a) Summary of the sedimentology and stratigraphy of the Wykeham sequence with the lithofacies and Wykeham unit codes discussed in the text. Mean ages from the P_Sequence age-depth model (Figure 3) are included for reference. b) core images of the lithofacies coupled with the key for the stratigraphy used in a). c) A cross-polarised thin-section image from TS-2 in WU-2c, illustrating the high numbers of calcified charophyte thalli in LF 2 which comprise a significant proportion of the carbonate content through the sequence (Appendix A).

Calcium carbonate content of sediment samples was determined using a Bascomb calcimeter (Gale and Hoare, 1991). Repeat measurements were undertaken every 10 samples to check for measurement consistency. Carbonate content is expressed as the % dry weight of the sample. Organic content was determined via the loss-on-ignition (LOI) method following Dean (1974). The percentage of siliclastic content was calculated as 100 – (carbonate content + organic content) of each sample. Thin section analysis was used to describe and interpret sedimentological changes of carbonate fabrics through the core sequence, and to guide bulk

sediment isotopic analysis. Thin section samples were prepared using the standard procedure of Palmer et al. (2008) and described following the terminology and protocol of Bullock et al. (1985). Full thin section descriptions and interpretations are presented in Appendix A.

Macrofossil analysis was undertaken on 2 cm thick samples between 680 and 100 cm to identify key taxa to reconstruct the lake's evolution, and to provide material for radiocarbon dating (section 3.2). Sample volume was measured by the displacement of water in a measuring cylinder (Birks, 2002). Sediments were sieved over a 125 µm mesh, with sodium pyrophosphate ($Na_4P_2O_7$) added to the sediment when necessary to aid disaggregation. Macrofossils were identified and counted using a stereo light microscope at between x10 and x40 magnification, using the reference collection at Royal Holloway, University of London, and identification guides (Berggren, 1964; Birks, 1980; van Geel *et al.,* 1980; 1989; Watson, 1981; Smith and Smith, 2004; Cappers *et al.,* 2006; Mauquoy and van Geel, 2007). Incomplete and/or very abundant remains such as mosses, leaf and wood fragments, and *Chara* thalli, were assigned a value on a 5-point, abundance scale (Birks and Matthewes, 1978; Birks, 2002; termed as AB), ranging from absent=0, present=1 (n=1-10), rare=10 (n=10-25), frequent=25 (n= 25-50), abundant=50 (n=50-100), very abundant= 100 (n=>100). Macrofossil counts are standardised to numbers per 50 cm^3 of sediment.

Bulk sediment $\delta^{18}O$ and $\delta^{13}C$ analysis was conducted on samples between 674 and 339 cm, where micromorphological analysis showed that carbonate was derived almost entirely from micrite and microspar crystals deposited either around charophyte thalli, or within a carbonate-rich matrix (section 4.1; Appendix A), and is consistent with authigenic carbonates precipitated within a lake body (e.g. Tye et al., 2016). No samples were taken from above 339 cm as the sedimentological and micromorphological analysis indicated that carbonate was present in very low abundances and was derived from detrital material including local limestone clasts. Contaminant carbonate fabrics (limestone clasts, charophyte thalli casts, ostracod carapaces and gastropod shells) were removed from the samples using fine forceps under a stereo light microscope, before being rinsed over 200 µm and 64 µm meshes to remove any remaining contaminant fabrics. The <64 µm fraction was immersed in 10 % H_2O_2 to remove organic material, and then air-dried and powdered. A Mettler Toledo XP6 microbalance was used to weigh samples to between 600-1200 µg and $\delta^{18}O$ and $\delta^{13}C$ values were determined using a VG PRISM series 2 mass spectrometer at Royal Holloway, with internal (RHBNC) and external (NBS19, LSVEC) standards run every 4 and 18 samples respectively. All isotope values are expressed as ‰ V-PDB. Internal precision produces mean analytical uncertainties of ± 0.04 ‰ for $\delta^{18}O$ and ± 0.02 ‰ for $\delta^{13}C$.

3.2. **Radiocarbon-based chronology**

Accelerator mass spectrometry (AMS) derived radiocarbon ages were obtained from terrestrial plant macrofossil samples from the Wykeham sequence (Table 1). Sample preparation followed that for the macrofossil samples (section 3.1), with remains picked using fine metal forceps into glass vials, filled with 2 ml of 10 % HCl, topped up with deionised water, and refrigerated to prevent mould growth.

Radiocarbon activity of the samples was determined at the Oxford Radiocarbon Accelerator Unit (ORAU), at the University of Oxford, the Scottish Universities Environmental Research Centre (SUERC), and the University of California, Irvine (UCI) following standard acid-base-acid pre-treatment and analytical procedures (Brock et al., 2010).

Table 1. Radiocarbon dates from the Wykeham sequence used to construct the age-depth model shown in Figure 3. $\delta^{13}C$ ranges for the dates support their terrestrial identification and that their radiocarbon age ranges would not be affected by substantial reservoir ages (e.g. Lowe et al., 2019). Posterior outlier values from the applied General outlier model are also listed, demonstrating coherent age depth relationships for all but three of the dates (OxA-32441, OxA-32434, and SUERC-84464).

Depth (cm)	Lab ID	Material	$\delta^{13}C$ (‰)	Radiocarbon date (BP)	Calibrated mean ± σ (cal a BP)	Outlier model posterior probability (%)
200-198	OxA-32343	*Betula* undiff. leaf fragments	-29.5	9925 ± 50	11360 ± 100	4
234-231	OxA-32397	Twigs (undiff.)	-29.1	10205 ± 45	11910 ± 95	2
281-279	SUERC-84465	Twigs (undiff.) and *B.nana* leaf fragments.	-28.2	11036 ± 45	12901 ± 71	100
305-301	SUERC-84464	*Betula nana* and Asteraceae seeds, x2, *S.herbacea* leaf fragments and twigs undiff.	-27.6	10594 ± 43	12581 ± 61	1
313-308	SUERC-84459	*Salix herbacea,* and Ericaceae undiff. leaf fragments	-28.6	10693 ± 44	12653 ± 38	1
347-345	OxA-32434	*Carex* achenes and *Betula* undiff. seeds	-28.1	11520 ± 45	13363 ± 48	98
376-374	OxA-32441	Twigs (undiff.)	-28.6	11540 ± 50	13376 ± 51	74
379-377	OxA-30541	*Carex* seeds with perigynium	-27.1	11210 ± 140	13060 ± 147	3
400-398	OxA-30030	*Carex* seeds	-28.9	11475 ± 45	13327 ± 54	2
417-413	OxA-32401	Twigs (undiff.)	-27.9	11420 ± 50	13257 ± 61	28
446-444	OxA-32436	*Juniperus communis*. needles, leaf frags. (undiff.)	-26.5	11895 ± 50	13696 ± 73	2
480-478	OxA-32437	*B.nana* leaf frags and twigs (undiff.)	-27.2	12320 ± 55	14325 ± 161	3
481-480	OxA-32435	Twigs (undiff.) and *B.nana* leaves	-26.9	12340 ± 50	14359 ± 161	2
554-550	SUERC-84458	*Betula nana* leaves, fruits, budscales, catkin scales and undifferentiated twigs	-29.5	12603 ± 48	14955 ± 128	14
592-586	SUERC-84457	*Potentilla erecta, Saxifraga* undiff. seeds, *Betula* undiff. catkin scale and undiff. leaf fragments	-23.7	12560 ± 50	14871 ± 158	4
636-633	SUERC-84456	Twig, leaf fragments undiff., *Cerastium* sp. and *Taraxacum* seeds	-27.3	12509 ± 47	14747 ± 187	36
641-636	UCIAMS-216468	*Poaceae* seeds, *Taraxacum* seed and twigs undiff.		12500 ± 40	14729 ± 181	43

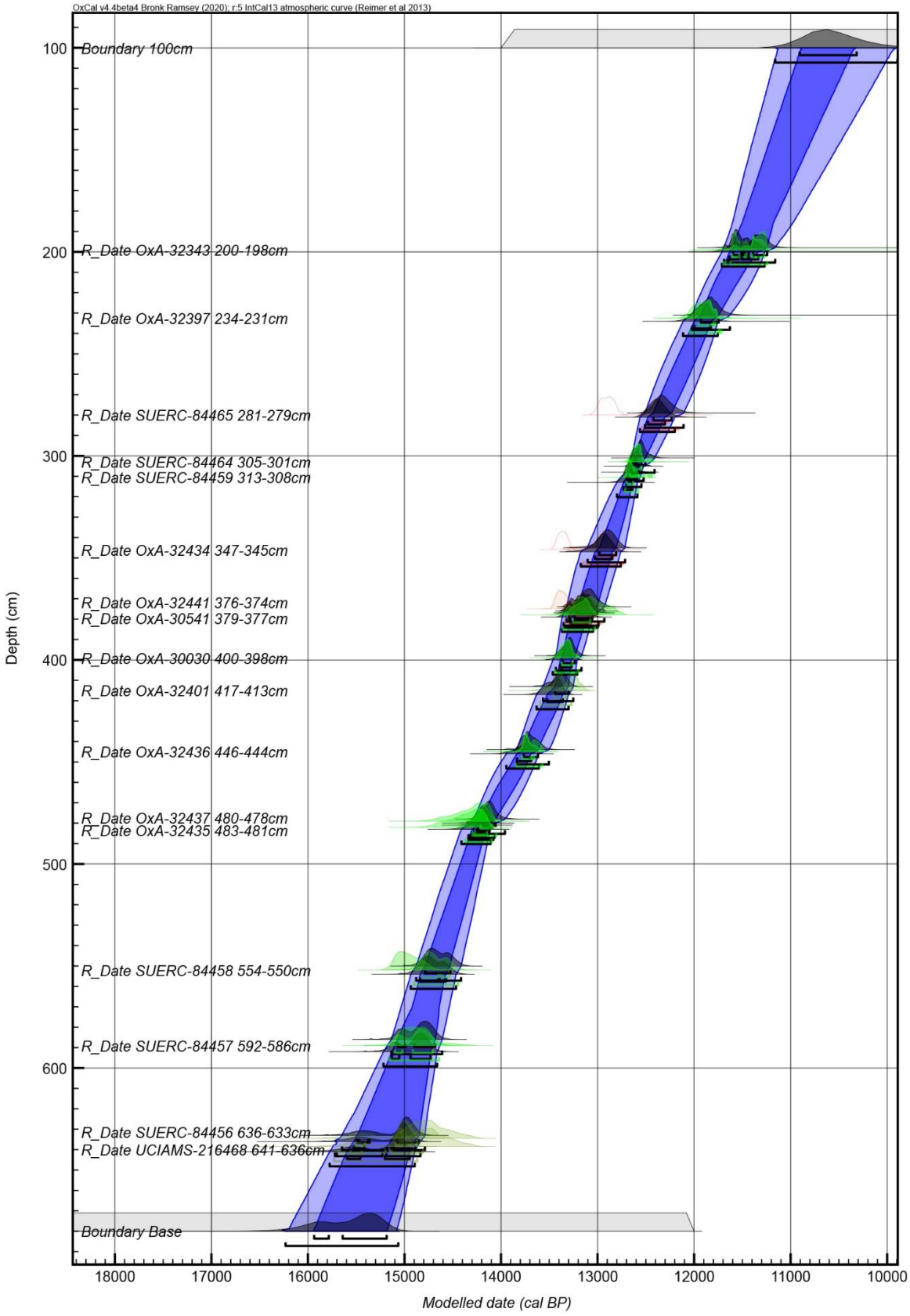

Figure 3. OxCal Bayesian age-depth model from the Wykeham sequence. The dark and light blue envelopes illustrate the 68 % and 95 % confidence intervals, respectively. Age ranges are coloured according to their posterior outlier probabilities (green = low, red= high; Table 1).

A Bayesian age-depth model was constructed using a *P_Sequence* deposition model in OxCal v4.4 (Bronk Ramsay, 2008; *in preparation*) using the IntCal13 calibration curve (Reimer et al., 2013). The model was run using a variable k factor, allowing the program to objectively determine the model rigidity in order to account for variations in sedimentation rate, and to obtain optimal age-depth relationships (Bronk Ramsey and Lee, 2013). Outlier analysis was performed to objectively down-weight any radiocarbon determinations deemed more likely to be erroneous, applying the 'General' outlier model with a prior outlier probability of 5% to each radiocarbon sample (Bronk Ramsey, 2009). These parameters produced a coherent age model for the sedimentary sequence (Figure 3; Appendices B and C). Three significant outliers (outlier posterior values >70%) were identified from the Outlier model (OxA-32441, OxA-32434, and SUERC-84464; Table 1). These samples contain either poorly preserved *Carex* achenes and/ or twigs which, in some instances, have the potential to produce erroneously older ages via reworking prior to final deposition (e.g. Turney *et al.,* 2000; Walker *et al.,* 2003). Sedimentological data from the dated strata support this interpretation, showing evidence for high levels of allogenic inwash (section 5.1), which may have eroded and re-deposited pre-existing organic deposits surrounding the basin (section 5.2). Modelled ages are reported as mean values ± σ ka BP, and the age model coding and output, including 68.2 % and 95.4 % ranges are included in Appendices B and C respectively. The age-depth model ranges from 15.59 ± 0.32 cal ka BP at 680 cm to 10.56 ± 0.31 cal ka BP at 100 cm (Figure 3).

3.3. **Reconstructing past lake-levels**

The principal control on temperate lowland lake levels are rates of groundwater recharge. controlled via rates of catchment precipitation (P) and evaporation (E) (Battarbee, 2000; Cohen, 2003). High lake-levels represent a positive P-E balance, whilst lower lake-levels represent a negative P-E balance (Harrison and Digerfeldt, 1993; Magny, 2007). The Wykeham palaeolake was formed in a topographic depression within permeable glacifluvial sediments and therefore the palaeolake level reflects the eastern VoP groundwater elevation which is controlled principally by meteoric recharge (Carey and Chadha, 1998; Brown et al., 2011). Therefore, variations in the palaeolake level reflect shifting rates of P and E, with high (low) lake levels invoking increased (decreased) rates of groundwater recharge under relatively humid (arid) hydroclimates.

Palaeolake-levels were reconstructed using the sedimentological, macrofossil, and isotopic datasets, which together show evidence for shifts from littoral (high) to eulittoral (low) conditions through the LGIT, a process that can be separated from hydroseral succession by the revertence to littoral conditions expressed in the overlying sediments. High relative lake-level phases are reconstructed using the following lines of evidence: a) littoral lithofacies

indicating deposition within a standing water body, b) macrofossil assemblages dominated by aquatic flora and fauna, c) carbonate $\delta^{13}C$ values between +3 and -3 ‰, indicative of lacustrine carbonates (Talbot, 1990), and d) no co-variance between carbonate $\delta^{18}O$ and $\delta^{13}C$, indicating an open lake system. Low relative lake-level phases are reconstructed using: a) eulittoral lithofacies, b) macrofossil assemblages dominated by eulittoral taxa, c) co-varying rises in carbonate $\delta^{18}O$ and $\delta^{13}C$ values (section 5.3), d) $\delta^{13}C$ values lower than -3 ‰, indicating shallow/paludal water bodies with high throughflow (Talbot, 1990; Candy et al., 2015).

Table 2. Macrofossil water depth ranges used to reconstruct the maximum water depth. *P. filiformis* and *P. pusillus* ranges derive from Spence and Chrystal (1970) and Dieffenbacher-Krall and Haltemann, (2000) respectively. All other ranges are derived from Hannon and Gaillard (1997).

Taxa	Water depth ranges (m)
Chara thalli.	<4-6
Myriophyllum spicatum	1-5
Potamogeton filiformis	*<1.5*
Potamogeton pusillus	*<1.5*
Equisetum fluviatile	0-1
Phragmites australis	0-2
Typha latifolia	0-1
Juncus undiff.	0-1
Carex undiff.	0-1

With the exception of charophyte gyrogonites/ oospores, the seeds and fruits of most aquatic taxa are not widely dispersed from their parent plants, meaning that their presence in the macrofossil record represents the aquatic vegetation in close proximity to the sampling site (Zhao et al., 2006). The Wykeham basin is a first order lake with a restricted catchment, a single spring-fed river input of less than 300 m length and direct coupling to the surrounding slopes (Figure 1), supporting our inferences for local groundwater changes. Therefore, by using maximum depth niches of the aquatic and wetland macrofossil taxa (Hannon and Gaillard, 1997), an estimate of the maximum water depth at the sampling site can be calculated and used to estimate shifts in the maximum groundwater elevation (Table 2). The results were constrained to altitudinal data using core depths and absolute altitudinal benchmarks (the Wykeham sequence extends between 19.56 and 25.38 mOD, 6.80 to 1.00 m below the contemporary land surface). An upper groundwater level constraint of 25.50 mOD was employed as no subaqueous deposits have been identified above this elevation in the Wykeham basin, elsewhere in Wykeham Quarry (Lincoln et al., 2017), or at Palaeolake Flixton (Taylor, 2011; Palmer et al., 2015). The final lake-level reconstruction was linearly detrended to permit a comparison throughout the period as accommodation space was lost from the basin as it infilled.

4. Results

4.1. Stratigraphy

The Wykeham basin sedimentary sequence is composed of four lithofacies (LF 1-4) consisting of interbedded carbonate-rich silty sands, peats and siliclastic-rich silts, sands and gravels (Table 3 and Figure 2). Using the sedimentology, plant macrofossil, and stable isotope results, and the age-depth model (section 3.1-3.2), the sequence is divided into 8 units (WU-1-8; Figure 2), which are described below.

Table 3. Summary of the lithofacies in the Wykeham sequence.

Lithofacies (LF)	LF codes	Description	Process interpretation	Depositional environment
1	Sm	Medium to fine minerogenic sand with isolated gravel clasts	Gravity flows in shallow water	Unstable gravel margins on the sides of depressions causing gravity flows into shallow water bodies: **Littoral**
2	Fm, Fl, Sm	Carbonate-rich massive to faintly laminated silty, friable fine sand with abundant carbonate thalli casts of *Chara sp.,* isolated gastropod shells and fine gravel clasts (Apoendix 1).	Still-slow-flowing water authigenic sedimentation in base-rich lakes	Spring-fed freshwater charophyte meadows on littoral lake benches (<4-6 m mean water depth): **Littoral**
3a	Fm; Sm;	Siliclastic-rich sandy clayey silt interbedded with laminations to beds of fine to coarse sands	Low energy suspension settling of allogenic material in shallow water depths	Shallow oligotrophic water-bodies with limited vegetation cover in either the catchment or within the lake: **Littoral**
3b	Sm: Gm	Siliclastic-rich fine-coarse sands and moderately to poorly sorted fine to medium gravels including limestone.	High energy inflows either via gravity flows or slumping of gravels from unstable basin margins during intervals of low relative lake-level	High energy and unstable catchment conditions in the absence of perennial standing water: **Eutlittoral/ Terrestrial**
4	C; Fm	Poorly to well humified silty peat irregularly interbedded with LF 2	Marginal accretion of organic detritus either where peat was submerged for long periods (poorly humified), or at higher elevations, being predominantly sub-aerially exposed (well humified)	Eulittoral marsh/ backswamp environments (< 1 m mean water depth) at the margins of water bodies: **Eulittoral**

4.2. WU-1 (680-676 cm; 15.59 ± 0.32 to 15.55 ± 0.31 cal ka BP)

WU-1 is the basal unit of the Wykeham sequence and is comprised of well- to moderately sorted, sand-rich siliclastic material, with gravel clasts including oolitic limestone (LF 1). The deposits are comprised principally of siliclastic content (57 %), whilst carbonate and organic content is comparatively low compared to the overlying strata (< 40 % and 3 % respectively). A single macrofossil sample obtained from WU-1 contained only charophyte oospores (Figure 4). No additional proxy data was obtained from these deposits.

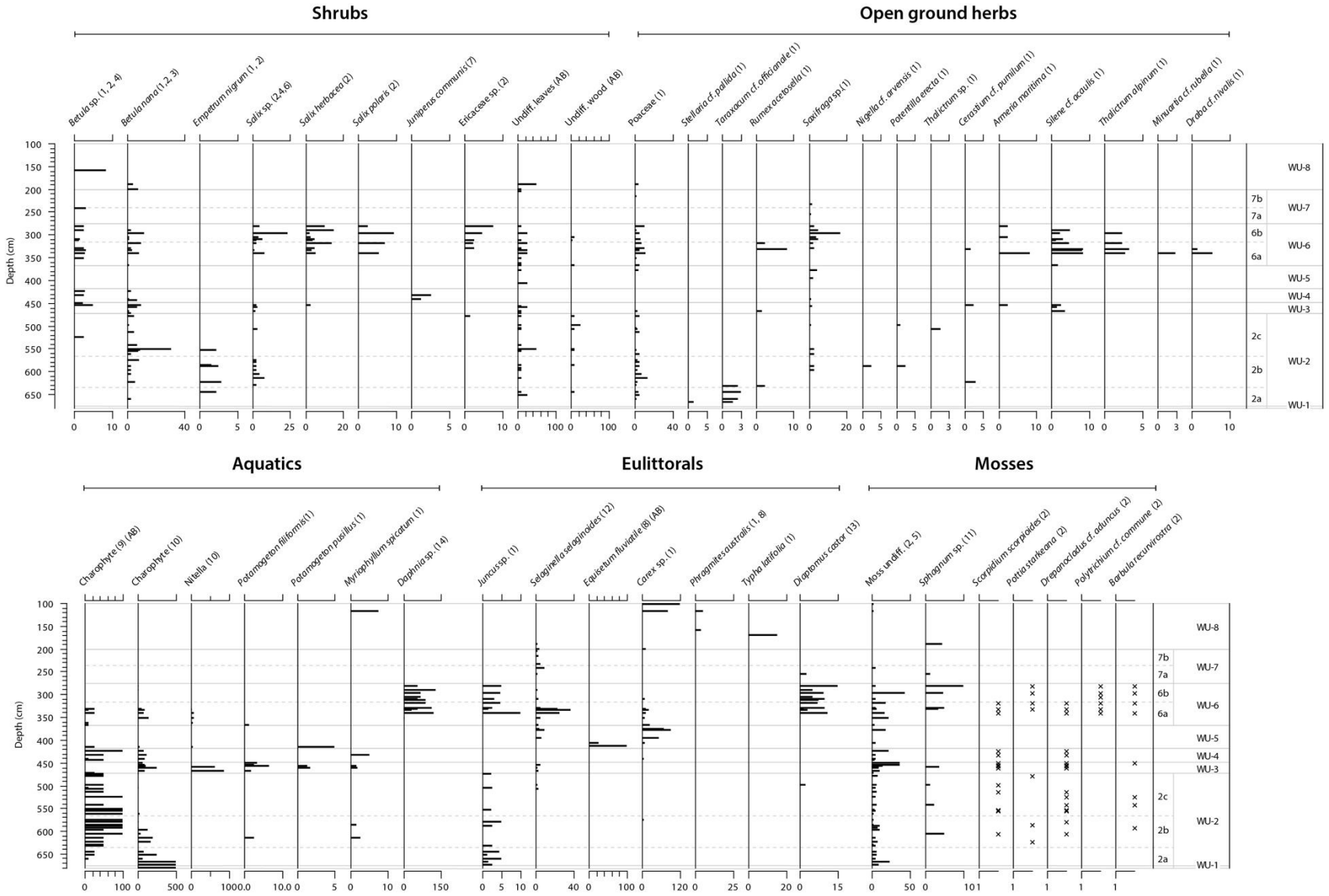

Figure 4. Macrofossils from the Wykeham sequence. (1) seeds/ fruits/ achenes, (2) leaves, (3) catkins, (4) twigs, (5) stems, (6) budscales, (7) needles, (8) rhizomes, (9) calcified thalli, (10) gyrogonites/ oospores, (11) sporangia, (12) megaspores, (13) egg sacs, (14) ephippia. (AB) denotes taxa counted using the abundance scale (section 3.1).

4.3. **WU-2 (676-472 cm; 15.55 ± 0.31 to 14.05 ± 0.09 cal ka BP)**

WU-2 is divided into three sub-units WU-2a (676-638 cm; 15.55 ± 0.31 to 15.20 ± 0.26 cal ka BP), WU-2b (638-568 cm; 15.20 ± 0.26 to 14.78 ± 0.13 cal ka BP) and WU-2c (568-472 cm; 14.78 ± 0.13 to 14.05 ± 0.09 cal ka BP) based upon the proxy results. WU2a consists of well-sorted carbonate-rich silty sands containing high abundances of calcified charophyte thalli encrustations (LF 2) that make up the rest of WU-2a-2c (674-472 cm). Carbonate (siliclastic) content fluctuates between 33 and 83 % (15 and 64 %) in WU-2a-2b, steadily rising (lowering) through these units. In WU-2c, carbonate content is consistently high (>70 %, reaching peak values of 82 %) and siliclastic content is low (15-30 %). Organic content is low throughout WU-2 (< 4 %). The WU-2 thin sections show that carbonate content is derived principally from micrite crystals within the sediment matrix and microspar crystals precipitated around charophyte thalli (Appendix A).

The aquatic macrofossil assemblage from WU-2 is dominated by two types of charophyte remains (Figure 4). In WU-2a, charophyte oospores dominate the aquatic assemblage but are replaced by calcified charophyte thalli casts in WU-2b which dominate the assemblage through the rest of WU-2. Other aquatic macrofossils consist of littoral taxa including *Potamogeton filiformis* and *Myriophyllum spicatum* seeds which are present in low numbers in WU-2b. Eulittoral species diversity is low, consisting entirely of *Juncus* undiff. seeds and moss leaves and stems including *Drepanocladus, Scorpidium scorpioides* and *Barbula recurvirostra*. Terrestrial remains consist of perennial herbs (Poaceae, *Taraxacum cf. officianale, Rumex acetosella, Potentilla erecta*) and dwarf shrubs (*Empetrum nigrum, Betula nana* and *Salix* undiff.).

$\delta^{18}O$ values are low at the base of the sequence but rise by +1.46 ‰ to -6.32 ‰ in WU-2a (Figure 5). In WU-2b, $\delta^{18}O$ values initially oscillate from -6.32 ‰ to -7.51 ‰, and then remain high and stable ($\delta^{18}O$ mean = -6.65‰, 1σ = 0.12‰) before steadily declining from -7.27 ‰ to -7.78 ‰ in WU-2c. $\delta^{13}C$ values are initially high (enriched) in WU-2a (+1.32 ‰) and become steadily lower (more depleted) through WU-2b-2c, reaching a minimum value of -2.50 ‰ at 478 cm. There is no co-variance between $\delta^{18}O$ and $\delta^{13}C$ values in WU-2 (r^2= 0.03).

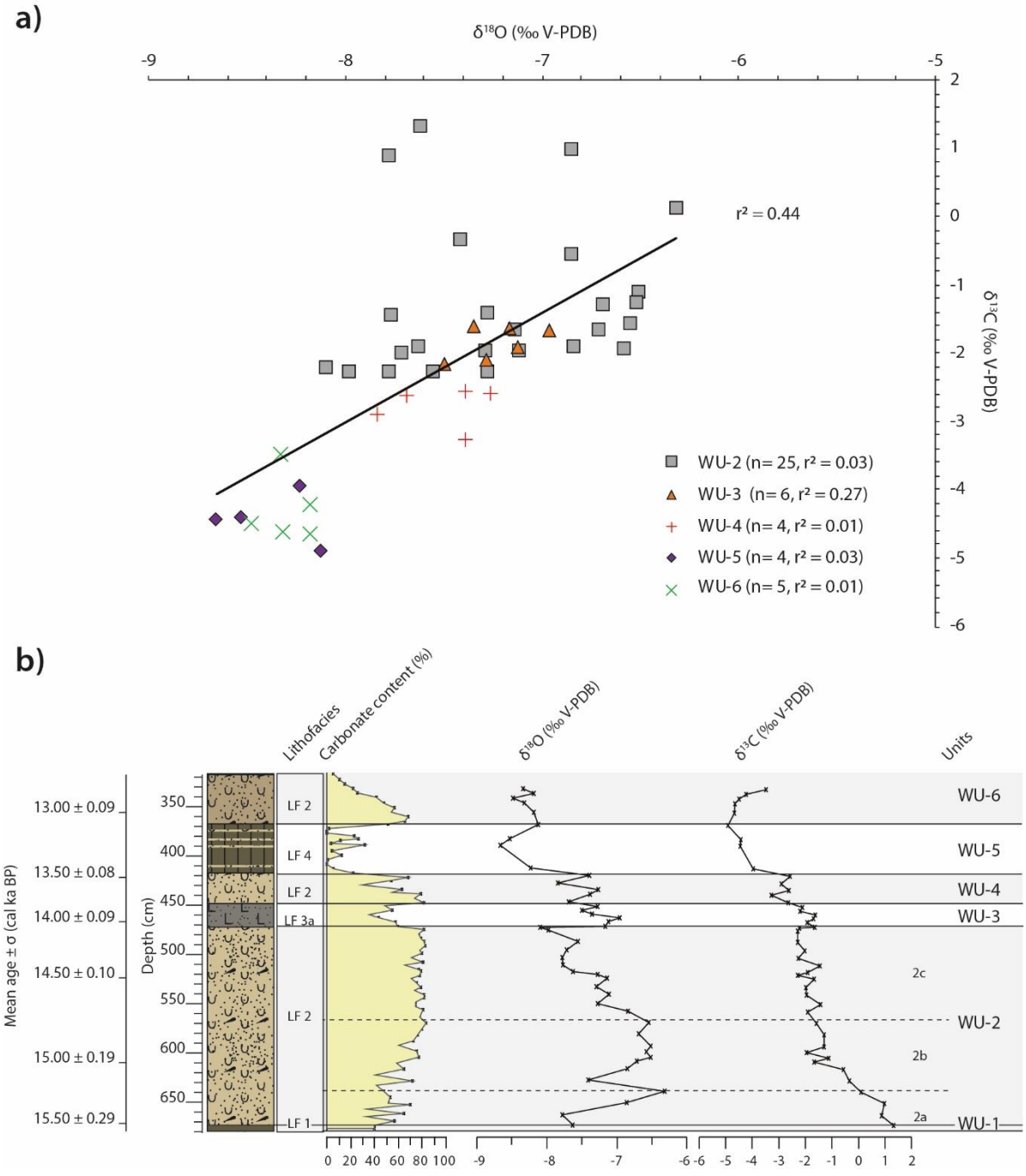

Figure 5. a) Comparison of the $\delta^{18}O$ and $\delta^{13}C$ values from the Wykeham sequence. b) Stratigraphic plot of the $\delta^{18}O$ and $\delta^{13}C$ values illustrating the lithofacies, stratigraphy and carbonate content through the sequence (from Figure 2) and the Wykeham units. Note that WU-6b, WU-7, and WU-8 are not displayed as no isotopic samples were taken from these units.

4.4. **WU-3 (472-448 cm; 14.05 ± 0.09 to 13.79 ± 0.08 cal ka BP)**

WU-3 is characterised by well-sorted, siliclastic-rich, fine sandy silts with isolated gravel clasts and moss-rich laminae (LF 3). Carbonate (siliclastic) content is lower (higher) than WU-2b and 2c (carbonate mean = 50 %, siliclastic mean = 46 %). Organic content remains low (<10 %) through WU-2 (Figure 2a). Charophyte thalli casts are also absent from the WU-3 aquatic macrofossil assemblage and are replaced by charophyte gyrogonites and littoral taxa

including *Potamogeton filiformis, Potamogeton pussilus* and *Myriophyllum spicatum*. Wetland/ damp ground taxa consist of clubmoss megaspores (*Selaginella selaginoides*) and other moss remains (including *Drepanocladus* undiff.). Terrestrial taxa consist of *Betula nana*, *Salix* sp., and upland perennial herbs including *Silene cf. acaulis., Rumex acetosella,* and *Armeria maritima*. $\delta^{18}O$ and $\delta^{13}C$ isotopic values become more enriched at the base of WU-3 and remain consistently more enriched than the mean isotopic values in WU-2c ($\delta^{18}O$ mean = -7.33‰, 1σ = 0.20‰; $\delta^{13}C$ mean = -1.97‰, 1σ = 0.28‰). The isotopic values also exhibit higher co-variance than the other Wykeham units (r^2 = 0.27) although this is based upon a relatively small sample size (n=6). Co-variance is further enhanced when including the uppermost WU-2c isotopic samples (r^2 = 0.57 between 475 and 451 cm) demonstrating that it is driven largely at the point of $\delta^{18}O$ and $\delta^{13}C$ enrichment between WU-2 to WU-3.

4.5. **WU-4 (448-417 cm; 13.79 ± 0.08 to 13.46 ± 0.08 cal ka BP)**

WU-4 consists of well-sorted silty sands containing high abundances of calcified charophyte thalli encrustations (LF 2) similar to those in WU-1. The deposits are carbonate-rich (30 to 80 %, mean = 58 %) whilst organic content is higher than in underlying deposits, reaching maximum values of 32 %. Siliclastic content is lower than WU-3 but rises from 15 % to 46 % through the unit. The aquatic macrofossil assemblage in WU-4 is dominated by charophyte thalli with only a single horizon also containing *M.spicatum* seeds at the top of the zone. Wetland/ eulittoral taxa are predominantly absent from WU-4, with only low numbers of trigonous *Carex* achenes recorded at 441 cm. Terrestrial remains consist principally of shrub species including *Juniperus communis* needles (present at the base of the zone), *Betula nana* fruits and *Betula undiff*. twigs and fruits (which in some instances appear hybridized). $\delta^{18}O$ and $\delta^{13}C$ isotopic values in WU-4 are more depleted than those in WU-3 ($\delta^{18}O$ mean = -7.53 ‰, 1σ = 0.13 ‰; $\delta^{13}C$ mean = -2.77‰, 1σ = 0.30 ‰) and do not co-vary (r^2 = 0.01).

4.6. **WU-5 (417-367 cm; 13.46 ± 0.08 to 13.07 ± 0.10 cal ka BP)**

WU-5 consists of organic-rich silts and poorly humified herbaceous peats (LF 4) which are interbedded with thin (0.5-2 cm thick) carbonate-rich silty laminae (LF 2). Carbonate content varies between 0 and 32 %, whilst organic and siliclastic content reach peak values of 66 % and 67 %, respectively. Littoral aquatic macrofossil taxa are absent from WU-5, with the macrofossil assemblage comprising of mainly eulittoral taxa including *Equisetum fluviatile* rhizomes, *Carex* sp. achenes and pleurocarp mosses including *Scorpidium scorpioides*. Terrestrial species are limited to low numbers of poorly preserved *Betula* sp. fruits, Poaceae seeds, *Selaginella selaginoides* megaspores, and perennial herbaceous taxa, including *Silene* cf. *acaulis*. $\delta^{18}O$ and $\delta^{13}C$ isotopic values from the LF 2 laminae within WU-5 are more

depleted than underlying deposits ($\delta^{18}O$ mean = -8.39 ‰, 1 σ = 0.25 ‰; $\delta^{13}C$ mean = -4.43 ‰, 1 σ = 0.39 ‰) and do not co-vary (r^2 = 0.03).

4.7. **WU-6 (367-276 cm; 13.08 ± 0.10 to 12.29 ± 0.10 cal ka BP)**

Based upon lithofacies changes, WU-6 is split into two sub-units (WU-6a-WU-6b). WU-6a (367-317 cm; 13.08 ± 0.10 to 12.72 ± 0.06 cal ka BP) consists of well-sorted carbonate-rich silts and sands (LF 2) that are overlain by WU-6b (317-276 cm; 12.72 ± 0.06 to 12.29 ± 0.10 cal ka BP), which consists of well-sorted silt-sand-rich siliclastic deposits with (0.5-2 cm thick) fine sand laminae and infrequent fine gravel clasts (LF 3) between 317 and 276 cm. Carbonate content steadily declines through WU-6a (from 68 % to 10 %) and remains below 10 % in WU-6b. Siliclastic content mirrors the carbonate content (increasing from 26 % to 94 % through WU-6a-6b) and organic content ranges between 2 % and 12 %.

Aquatic macrofossil taxa including calicified charophyte thalli casts and oospores re-appear at the base of WU-6. Calcified charophyte thalli, however, are only present within the basal 36 cm of the sub-unit, and are frequently broken before becoming absent above 331 cm. Aquatic fauna (*Daphnia* sp. epphipia and *Diaptomus castor*) are present sporadically at the base of the unit and increase in abundance above 340 cm as carbonate content declines < 30 % and siliclastic content increases to > 60 %. Low numbers of eulittoral taxa including *Carex* undiff.*,* *Juncus* undiff., and *Sphagnum* undiff. sporangia are recorded throughout WU-6. Terrestrial macrofossil remains are composed principally of open ground herbs (Poaceae, *Saxifraga cf. granulata*. *Silene cf. acaulis*, *Armeria maritima* and *Thalictrum cf. alpinum*), although *Betula* sp. remains (including *Betula nana*) and *Salix herbacea* (leaves and petioles) are also present in low frequencies. $\delta^{18}O$ and $\delta^{13}C$ isotopic values in WU-6a are depleted ($\delta^{18}O$ mean = -8.30 ‰, 1 σ = 0.12 ‰; $\delta^{13}C$ mean = -4.30 ‰, 1 σ = 0.49 ‰) and exhibit no co-variation (r^2 = 0.01). No stable isotopic samples were taken from WU-6b (section 3.1).

4.8. **WU-7 (276-200 cm; 12.29 ± 0.10 to 11.50 ± 0.13 cal ka BP)**

Based upon lithofacies changes, WU-7 is sub-divided into two sub-units (WU-7a-WU-7b). WU-7a (276-237 cm; 12.29 ± 0.10 to 11.95 ± 0.09 cal ka BP) consists of normally and reverse graded sands and fine gravels interbedded with medium to fine silty sands (LF 3b). Carbonate content ranges between 4 % to 19 %, which from thin section analysis reflects detrital limestone incorporated within the sand and gravel facies (section 3.3). Above 237 cm (WU-7b; 11.95 ± 0.09 to 11.50 ± 0.13 cal ka BP), deposits revert to well- to moderately sorted silt-sand-rich siliclastic material interbedded with fine to medium sands (0.5 to 2 cm thick). These deposits consist almost entirely of siliclastic content (> 80 %) with carbonate and organic content below 10 %. Macrofossil concentrations are low throughout WU-7 and identifiable

terrestrial macrofossils are confined to *Saxifraga* undiff. seeds and *Betula* sp. fruits which are poorly preserved. Wetland and aquatic species diversity in the macrofossil samples is also low, with only *Selaginella selaginoides* megaspores*, Juncus* undiff. seeds and *Chara* gyrogonites recorded. No stable isotopic samples were taken from WU-7.

4.9. **WU-8 (200-100 cm; 11.50 ± 0.13 to 10.56 ± 0.31 cal ka BP)**

WU-8 consists of organic-rich silt grading into poorly to moderately humified silty herbaceous peat above 194 cm (LF 4). Organic and siliclastic content rise from 10 % to over 80 % and fall from 90 % to 20 % respectively between 200 and 140 cm, whilst carbonate is absent throughout WU-7. Although no sediments were obtained above 100 cm, records from elsewhere in the palaeolake contain sediments analogous to WU-8 that extend to the contemporary land surface (Figure 1d). The macrofossil assemblage consists primarily of eulittoral taxa with a low species diversity (trigonous *Carex* achenes, *Typha latifolia*, and rhizomes of *Phragmites australis*). Terrestrial macrofossil remains are low in frequency and include *Betula nana* leaves and Poaceae seeds. Aquatic macrofossil taxa are absent from WU-8 with the exception of *Myriophyllum spicatum* seeds at 118 cm. No stable isotopic samples were taken from this unit.

5. Interpretation

5.1. **Sedimentology**

The Wykeham lithofacies reflect deposition within littoral lacustrine- (LF 1,2,3a) to eulittoral- (LF 3b, 4) lake marginal environments (Table 3). Charophyte-rich carbonates (LF 2) in WU-2-5a reflect sedimentation dominated by authigenic calcium carbonate precipitation upon a littoral lake bench slope in waters up to 4 to 6 m deep (Murphy and Wilkinson, 1980; Treese and Wilkinson, 1982). Low siliclastic and organic content in these deposits invokes a sub-aqueous depositional environment with limited allogenic inwash from the catchment and sedimentation dominated by carbonate precipitation around charophyte thalli and within the water column, as a consequence of photosynthesis in *Chara* meadows during summer months (McConnaughey, 1991; Hammarlund *et al.,* 2003). These sediments are characteristic of *Chara* marl lakes in the British Isles (Pentecost, 2009), and demonstrate precipitation within the groundwater-fed Ca-rich waters in the basin (section 3.3).

Siliclastic sands, silts, and clays (LF 1 and LF 3a) are indicative of low organic productivity within the water body and surrounding catchment, with fine-grained deposits falling from suspension during periods of limited turbulence in the water column (Palmer *et al.,* 2015). Coarse-grained siliclastic beds (LF 3b) are indicative of high energy processes delivering allogenic sediment into the topographic depression either via subaerial exposure and slumping of the basin margins (Ashley, 1975), and/or flood inflow events (Schilleref *et al.,*

2015) with limited organic content in either the depression or surrounding catchment. Coarse particle sizes and the lack of interbedded subaqueous deposits suggests that LF 3b represents phases of low relative lake-levels in the depression and the absence of perennial standing water (section 5.4).

Organic-rich silty peats (LF 4) represents deposition in close association with the mean water level in a eulittoral depositional environment. Interbeds of LF 2 in WU-5 suggests shifts in the relative lake-level, switching between eulittoral and littoral conditions. The steady increase in organic content in WU-8 invokes the final infill of the water body via hydroseral succession.

5.2. **Macrofossils**

Aquatic and eulittoral macrofossils in the Wykeham sequence represent vegetation growing within or at the margins of the palaeolake respectively (section 5.4). The terrestrial macrofossil assemblage reflects flora growing locally within the catchment and entering the palaeolake body either via direct airfall, or streamflow. The small size of the Wykeham basin and the stream inflow provide significant potential for the influx of terrestrial macrofossils into the basin. Low abundances of terrestrial macrofossils recovered in WU-5, WU-7, and WU-8 are interpreted to reflect a taphonomic bias during intervals of low relative lake-level and limited inflow (section 5.4). The macrofossils within these units therefore only reflect terrestrial taxa growing directly within or at the margins of the Wykeham basin.

The following trends are identified in the terrestrial macrofossil assemblage. In WU-2 and WU-3, the assemblage is characteristic of an open steppic landscape, with limited shrub cover (*Betula nana, Salix* sp. and *Empetrum nigrum*) in the VoP lowlands between 15.55 ± 0.31 and 13.79 ± 0.08 cal ka BP. Disturbed ground- and montane taxa (*Rumex acetosella* and *Silene c.f. acualis* respectively) in WU-3 suggest a temporary niche change between 14.05 ± 0.09 and 13.79 ± 0.08 cal ka BP, possibly in response to a deterioration in hydroclimatic conditions (section 5.5). Lower abundances of herbs and rises in shrubby taxa (e.g. *Juniperus communis*.) in WU-4 reflect the stabilisation of the landscape between 13.79 ± 0.08 cal ka BP and 13.46 ± 0.08 cal ka BP. The rise in *Betula* sp. remains in WU-4 reflects an expansion in local *Betula* growth in the catchment. No *Betula* remains in the Wykeham sequence can be conclusively assigned to tree species (e.g. *B. pubescens* or *B. pendula*) however, suggesting that for the duration of the Wykeham palaeolake's existence, closed forest cover did not develop in the eastern VoP (section 5.5).

The WU-6 and WU-7 assemblage indicates a change in the ecological niche and a re-opening of the catchment vegetation cover. Open ground herbs and shrubs tolerant of disturbed ground (e.g. *Rumex acetosella*), and late-lying snow cover (e.g. *Salix herbacea*) suggest a deterioration in climatic conditions (section 5.5) and the re-development of open disturbed

grassland environs around the Wykeham basin. High macrofossil concentrations in WU-6 coincide with rising allogenic inwash into the basin. Allogenic inwash would have led to enhanced erosion and redeposition of sediments and vegetation from the lake margins into the water body (section 5.1). These processes are thought to explain the apparently old radiocarbon ages from OxA-32441, OxA-32434, and SUERC-84464, redepositing *Carex* macrofossils and twigs from the basin margins (section 3.2). Low terrestrial macrofossil concentrations in WU-7 and WU-8 suggest low catchment vegetation cover during the terminal stages of the palaeolake.

5.3. **Stable isotopes**

5.3.1. $\delta^{18}O$

In temperate mid-latitude regions such as the British Isles, it is common to interpret changes in the $\delta^{18}O$ value of lacustrine carbonates as a change in the $\delta^{18}O$ of regional precipitation (Marshall et al., 2002, 2007; Candy et al., 2016; Blockley et al., 2018). This is because the $\delta^{18}O$ of lacustrine carbonates is strongly related to the $\delta^{18}O$ of the lake water that they precipitate from. In the British Isles, lake waters are rapidly recharged by groundwater, the $\delta^{18}O$ of which closely matches the $\delta^{18}O$ of mean annual rainfall (Darling and Talbot, 2003; Darling, 2004). Consequently, major shifts in the $\delta^{18}O$ of rainfall are quickly propagated through the $\delta^{18}O$ of groundwater into the $\delta^{18}O$ of lake water and, as a result, into the $\delta^{18}O$ of any resultant carbonate. As there is a close correlation in mid-latitude western Europe between the $\delta^{18}O$ of rainfall and the prevailing air temperature, the majority of researchers have interpreted shifts in the $\delta^{18}O$ of lacustrine carbonates in LGIT sequences as being primarily driven by air temperature changes (Marshall et al., 2002; Van Asch et al., 2012; Candy et al., 2016). The palaeolake carbonates at Wykeham are largely derived from photosynthesis within charophyte meadows (section 5.1), meaning that the $\delta^{18}O$ signal is likely to be weighted towards the spring to summer months when carbonate precipitation would be greatest (e.g. von Grafenstein et al., 2000). Whilst lake waters in the British-Isles are likely to be susceptible to evaporation, and hence isotopic modification that may affect the relationship with the isotopic connection to rainfall, the magnitude of this process is, in most instances, likely to be limited compared to the large- scale changes in air temperature/ $\delta^{18}O$ of rainfall that occurred across the LGIT. Using this rationale, the following patterns are identified in the Wykeham $\delta^{18}O$ sequence.

Rising values at the base of WU-2a representing ameliorating temperatures between 15.55 $\pm$ 0.30 and 15.20 $\pm$ 0.26 cal ka BP. High and stable $\delta^{18}O$ values between 15.20 $\pm$ 0.26 and 14.78 $\pm$ 0.13 cal ka BP (WU-2b) indicating carbonate precipitation occurring under high mean

480 temperatures before a steady decline in $\delta^{18}O$/ temperatures between 14.78 ± 0.13 and 14.05
481 ± 0.09 cal ka BP (WU-2c). Co-varying enrichment in $\delta^{18}O$ and $\delta^{13}C$ values in WU-3, coupled
482 with sedimentological and macrofossil evidence for a decrease in lake-level suggest either: a)
483 a temporary hydrological closure of the lake under more arid hydroclimates (Talbot, 1990), b)
484 a shift in regional hydroclimate (Drummond et al., 1995; Leng and Marshall, 2004), and/ or, c)
485 enhanced allogenic inwash of $\delta^{18}O$ and $\delta^{13}C$ enriched geological carbonates from the
486 catchment (Candy et al., 2015) between 14.05 ± 0.09 and 13.79 ± 0.08 cal ka BP (section
487 5.4). A decline in $\delta^{18}O$ values in WU-6 advocates deteriorating mean annual temperatures at
488 13.46 ± 0.08 cal ka BP (417 cm) which is maintained until the cessation of authigenic
489 carbonate deposition at *ca* 12.72 ± 0.06 cal ka BP.

490 These interpretations are corroborated by two lines of evidence: a) comparable $\delta^{18}O$ records
491 from sedimentary sequences pre-dating the Holocene at Palaeolake Flixton (Candy et al.,
492 2017), b) comparable palaeotemperature records from multiple British sequences (e.g. Walker
493 et al., 1993; 2003; Brooks et al., 2012) supporting the assertion that the changes in $\delta^{18}O$ at
494 Wykeham principally reflect local-regional temperature changes occurring in NE England
495 through the LGIT.

496 *5.3.2. $\delta^{13}C$*

497 The $\delta^{13}C$ values of authigenic lake carbonates reflects the ^{13}C of dissolved inorganic carbon
498 (DIC) in the lake water, which in turn relates to the DIC of spring and groundwater recharging
499 the lake, biological activity within the lake basin, and the equilibration of CO_2 between the lake
500 water and the atmosphere (Talbot, 1990; Leng and Marshall, 2004; Candy *et al.,* 2016).

501 Declining $\delta^{13}C$ values through WU-2-4 (from -+1.32 to -2.80‰) reflects increasing supplies
502 of ^{13}C depleted in CO_2 in the lake DIC, driven by soil development in the lake catchment and
503 a lower influence of geologically derived $\delta^{13}C$ in the DIC signal (Hammarlund et al., 1997; Leng
504 and Marshall, 2004; Candy *et al.,* 2016). This is consistent with $\delta^{13}C$ trends from other LGIT
505 lake carbonate records in the British Isles (e.g. Marshall et al., 2002; Candy et al., 2016) and
506 is also supported by the Wykeham macrofossil evidence and palynological records from
507 neighbouring Palaeolake Flixton, and Gransmoor, where vegetation cover increases through
508 the Lateglacial Interstadial (Walker et al., 1993; Day, 1996; Abrook, 2017).

509 The $\delta^{13}C$ values in WU-5-6 are more depleted than typical lacustrine carbonates (i.e. between
510 -3 to +3‰; Talbot, 1990), and are representative of palustrine deposits formed in shallow pools
511 with short residence times and high rates of through flow (e.g. Candy et al., 2015). This is
512 supported by the lake-level change reconstructions from the other proxy data, which infer
513 shallow water depths (section 5.4). The shift towards depleted rather than enriched values in

WU-5 & 6 however, shows that the water body was not severely affected by evaporitic enrichment during carbonate precipitation, and remained an open system, likely due to the low residence time of the lake water in the basin.

5.4. **Lake-level changes**

The littoral lithofacies and high volumes of charophyte thalli in WU-2 and WU-4 are indicative of littoral bench slopes in perennial waters no deeper than 4-6 m (Murphy and Wilkinson, 1980; Treese and Wilkinson, 1982; Figure 6; Table 4). Low numbers of other shallow aquatic taxa suggest that WU-2 and WU-4 represent the deepest water facies in the sequence, with peak LGIT groundwater elevations (< 25.50 mOD) obtained between 13.79 ± 0.08 and 13.46 ± 0.08 cal ka BP (WU-3). At the base of the sequence (WU-1 to WU-2a), high volumes of charophyte gyrogonites/ oospores are indicative of high rates of sexual reproduction in shallow water depths (Soulié-Märsche and García, 2015) suggesting that during the initial stages of infill, the lake depth was low (< *ca* 2 m) and possibly susceptible to seasonal dessication, before rising to *ca* 23-24 m OD in WU-2a, perennially submerging the Wykeham depression and enabling clonal vegetative reproduction of the charophyte colonies (WU-2b). In WU-3, charophyte thalli are replaced by gyrogonites/ oospores coupled with *P.filiformis, P.pusillus* and *Myriophyllum spicatum*, advocating a temporary regression in the water depth to below 1.5 m (*ca* 23.20 mOD) between 14.05 ± 0.09 and 13.79 ± 0.08 cal ka BP (Spence and Chrystal, 1970; Dieffenbacher-Krall and Halteman, 2000). Eulittoral facies, coupled with the expansion of eulittoral macrofossil taxa in WU-5 and WU-8 show that the maximum mean water depth was below 1 m above the infill elevation (22.21-22.17 mOD and 24.38-25.38 mOD respectively) between 13.46 ± 0.08 and 13.08 ± 0.10 cal ka BP, and after 11.50 ± 0.13 cal ka BP, respectively. Using the macrofossil taxa alone, water depths are less well constrained in WU-6-7. Charophyte thalli in WU-6a are poorly preserved, and frequently fragmented (section 5.1; Appendix A), suggesting unstable conditions in the water column. *Diaptomus castor* egg sacs, moss remains, charophyte gyrogonites and depleted $\delta^{13}C$ values (section 5.3) all support shallow (< *ca* 2 m) and ephemeral waters susceptible to seasonal desiccation between 13.08 ± 0.10 and 12.72 ± 0.06 cal ka BP (Bennike, 1988; Talbot, 1990). Gravel facies in WU-7a (LF 3b) indicate intervals of minimal standing water, with the groundwater table lying below the infill elevation of the Wykeham basin (<23.62-24.01 mOD) between 12.29 ± 0.10 cal ka BP and 11.95 ± 0.09 cal ka BP. The re-introduction of sub-aqueous deposits in WU-7b indicate higher effective precipitation regimes in the VoP after 11.95 ± 0.09 cal ka BP but, with limited macrofossil evidence in these deposits, precisely constraining maximum water depths is not possible. The high and low lake-level phases identified in the Wykeham basin are consistent with other multiproxy based lake-level reconstructions at Wykeham Quarry (Lincoln et al., 2017), and lithostratigraphic reconstructions at Palaeolake Flixton (Palmer et al., 2015) which

were fed by the same groundwater source, supporting the interpretation that they represent changes in the P-E balance of the VoP groundwater aquifer.

Table 4. Summary of evidence used to reconstruct relative lake-level changes through the Wykeham sequence (section 5.4). Maximum mean water depth is derived from the macrofossil depth niches in Table 2. The water table elevation is calculated from the lake infill elevation + the maximum mean water depth to a maximum elevation of 25.50 mOD (see text).

WU-	Infill elevation (mOD)	Sedimentology	Dominant macrofossils	Stable isotopes	Maximum mean water depth (m)	Water table elevation range (mOD)
1	19.58-19.64	LF 1	Aquatics: charophyte gyrogonites	N/A	*ca* 2 m	
2a	19.64-20.00	LF 2: littoral facies	Aquatics: charophyte gyrogonites	No co-variance between $\delta^{18}O$ and $\delta^{13}C$ (open water body)	*ca* 4 m	21.64-23.92
2b	20.00-20.70		Aquatics charophyte thalli casts		*ca* 4 m	24.05-24.60
2c	20.70-21.66					24.70-25.50
3	21.66-21.90	LF 3a: littoral facies	Shallow aquatics: *P.pusillus, P.filiformis, M.spicatum*, absence of charophyte thalli casts	Moderate $\delta^{18}O$ and $\delta^{13}C$ co-variance. Evaporitic enrichment and/ or detrital contamination?	*ca* 1.5 m	23.17-23.38
4	21.90-22.21	LF 2: littoral facies	Aquatics: charophyte thalli casts	No co-variance between $\delta^{18}O$ and $\delta^{13}C$ (open water body)	*ca 4* m	*ca* 23.90-25.50
5	22.21-22.71	LF 4: eulittoral facies	Eulittorals: *Equisetum, Carex*	Depleted $\delta^{13}C$ invokes shallow, palustrine conditions	< 1 m	22.21-23.71
6a	22.71-23.21	LF 2: littoral facies	Aquatics-eulittorals: (*D.castor* suggest that standing water may have been ephemeral)		Estimated < 2 m	22.71-25.50
6b	23.21-23.62	LF-3a: littoral facies		N/A		
7a	23.62-24.01	LF 3b: eulittoral facies	No dominant taxa, absence of aquatics	N/A	<1 m	<23.62-<24.01
7b	24.01-24.38	LF-3a: littoral facies	Eulittorals: (*Carex*), low numbers of charophyte gyrogonites	N/A	0-2 m	<24.01-25.50
8	24.38-25.38	LF 4: eulittoral facies	Eulittoral and terrestrial taxa	N/A	<1 m	24.38-25.50

5.5. **Synthesis**

Between 15.59 ± 0.32 cal ka BP and 15.20 ± 0.26 cal ka BP, a topographic depression (kettle hole) enabled a shallow water body in the Wykeham basin to start to accumulate sediment (Figure 7). The basin itself probably formed from the melting of dead ice that remained after the deglaciation of the NSIL in the eastern VoP post *ca* 17.3 ka BP (Evans et al., 2017). The basal age range for the Wykeham sequence indicates that the dead ice here melted within a maximum of *ca* 2 ka. This age range is consistent with the initial infill of other kettle holes in N. Ireland (Watson et al., 2010) and S. Sweden (Wohlfarth et al., 2018), suggesting that dead ice melt and lake formation in the deglaciated outwash plains of the British Isles and Fennoscandia may have occurred in response to rising summer temperatures after ~16.0 cal ka BP, during the latter phases of Heinrich Stadial 1. Sedimentation in the Wykeham basin was initially dominated by allogenic material (WU-1), but as the water level increased, the lake was colonised by pioneering stands of charophytes which, when coupled with rudimentary perennial herbaceous communities (*e.g. Taraxacum cf. officianale*) and shrubs (e.g. *Empterum* nigrum) in the lake catchment, limited allogenic influx into the lake and facilitated the production of authigenic carbonate.

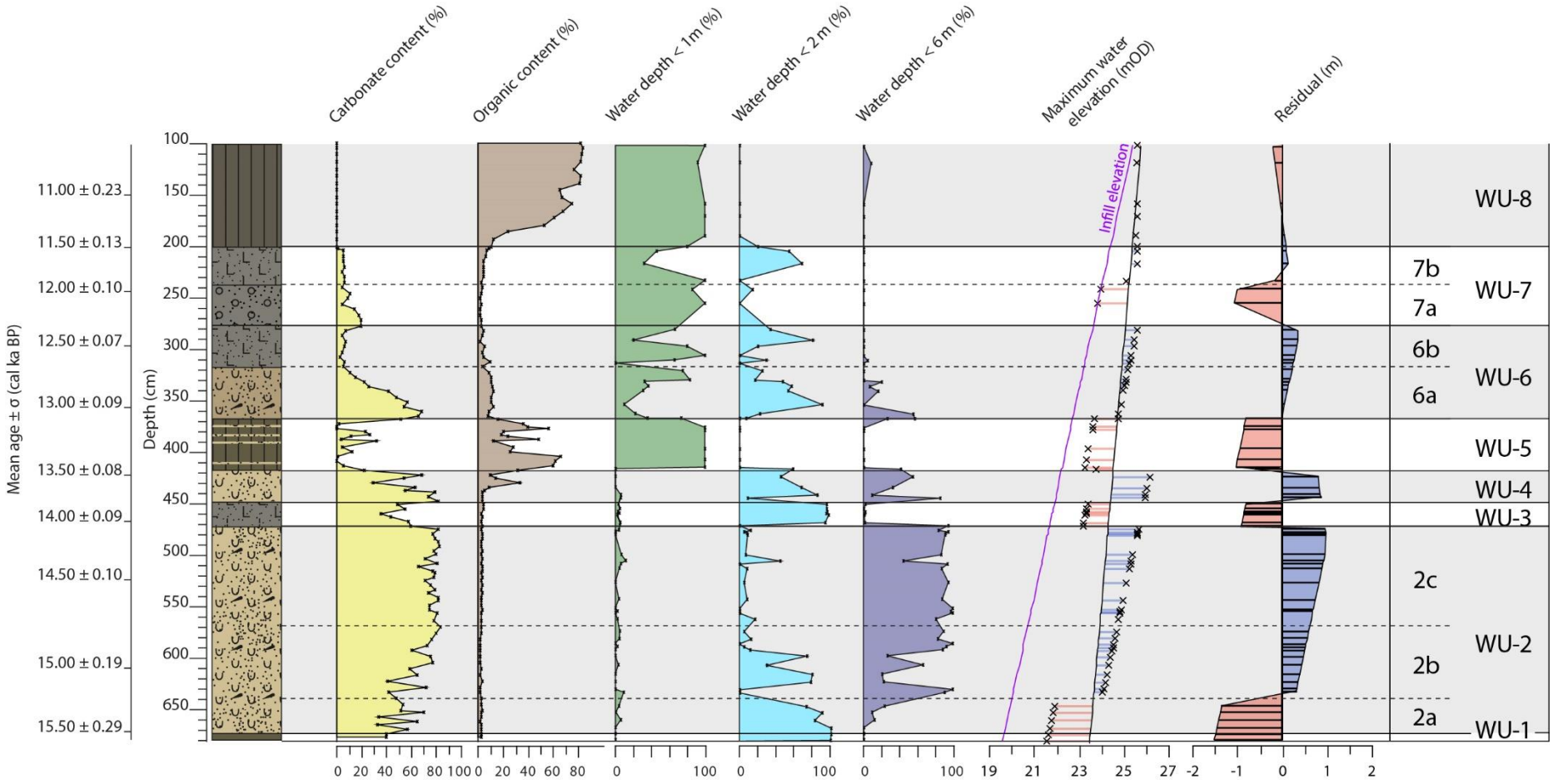

Figure 6 Summary of the sedimentary (lithofacies follows those of Figure 2), and ecological (<1 m, < 2 m and < 6 m water depth % are calculated from the niches of littoral-eulittoral macrofossil taxa summarised in Table 4) evidence used to reconstruct relative lake-level changes from the Wykeham sequence. Maximum water elevations (mOD) are calculated from the infill elevation of the Wykeham sequence + the optimum water depth niche of the littoral-eulittoral macrofossil assemblage. Positive residuals from a linear smoothing line (grey line) reflect high relative lake-level phases (in blue) and negative residuals (in red) reflect low relative lake-level phases. Mean ages ± σ from the age model (Figure 3) are included for reference

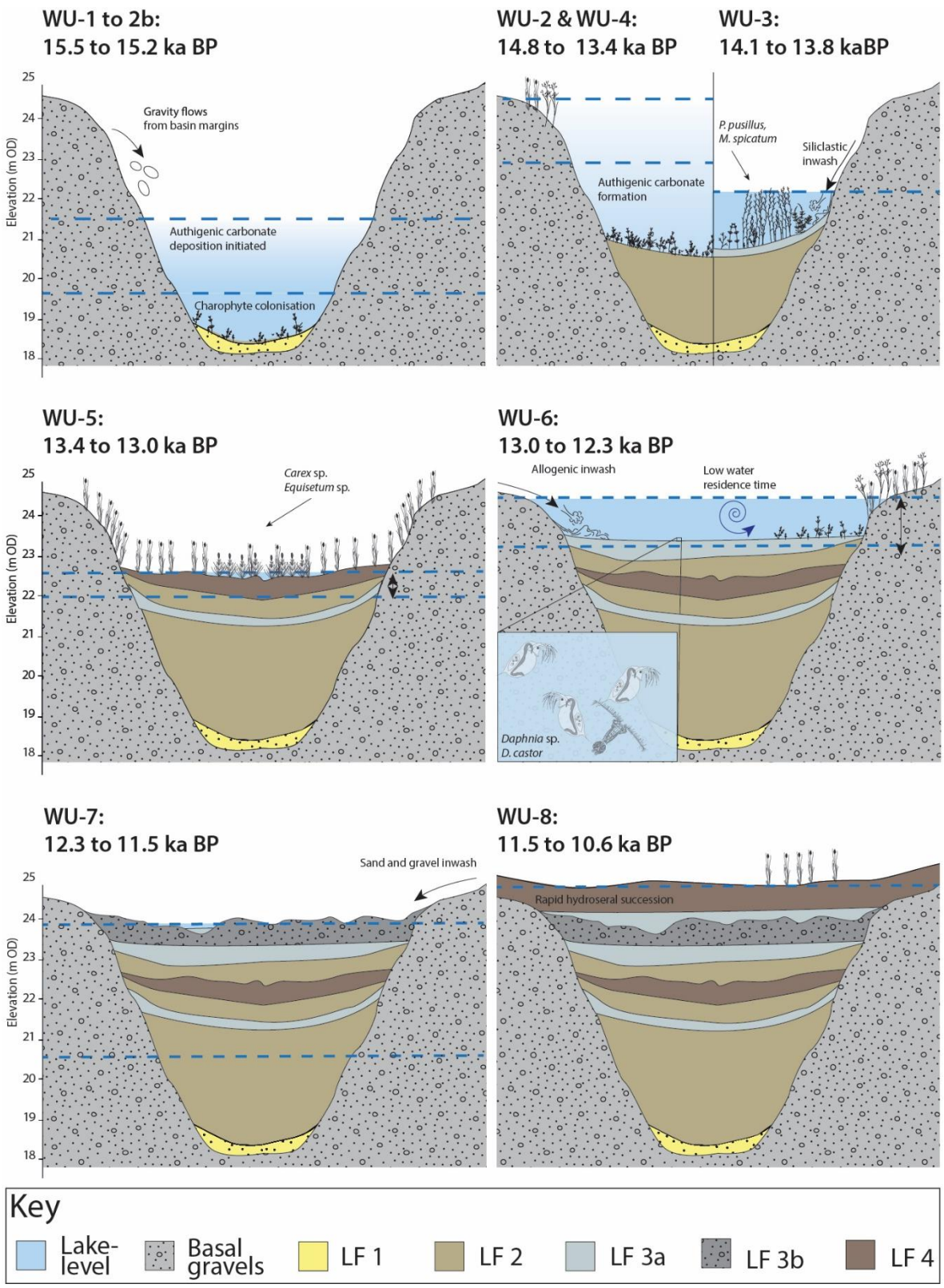

Figure 7. Schematic illustration of the hydrological evolution of the palaeolake based upon the proxy evidence from WU-1-8. Changes in the lake-level elevation are marked by dashed blue lines.

$\delta^{18}O$ from the Wykeham basin carbonates reflects a mean annual temperature signal weighted towards the summer months, when carbonate precipitation in the lake was greatest (section 5.3.1). High $\delta^{18}O$ values coupled with thermophilic macrofossil taxa (*M.spicatum, P.filiformis*) together show that summer temperatures were mild in the VoP between 15.20 ± 0.26 and 14.78 ± 0.13 cal ka BP (WU-2b). Similar 'early' spring-summer warming signals to those at Wykeham have also been identified elsewhere in the low and mid-latitudes of Europe (e.g. Genty et al., 2006; Watson et al., 2010; Wagner-Cremer et al., 2011; Samartin et al., 2012; Wohlfarth et al., 2018) suggesting that these hydroclimatic changes reflect an amelioration signal in the European latitudes between 16-15 cal ka BP (Figure 8; Blockley et al., 2004; Buizert et al., 2014; Landais et al., 2018).

At *ca* 14.65 cal ka BP, regional hydroclimatic regimes shifted across the N. Atlantic seaboard, causing hemispheric alterations in atmospheric circulation cells and ameliorations in mean annual and, in particular, winter temperatures at the start of GI-1e (Renssen and Isarin, 2001; Steffensen et al., 2008; Rasmussen et al., 2014). Declining $\delta^{18}O$ in WU-2c reflects either a shift in the seasonality of carbonate precipitation in the basin, driven by the amelioration in winter temperatures, reduced seasonal ice cover across the lake, and a lengthening of the summer months preferred for calcite precipitation, and/ or higher $\delta^{18}O$ depleted groundwater recharge of the water body via melting permafrost. Declining summer temperature (TMax) values from Gransmoor, however, suggest that the depletion in $\delta^{18}O$ in WU-2c is in part derived from declining air temperatures in NE England through the GI-1e chronozone (Walker et al., 1993; Blockley et al., 2004; Elias and Matthews, 2014). Vegetation cover in the VoP remained open during this interval, with perennial herbaceous communities continuing to persist in the Wykeham lake catchment (section 5.2), but decreasing $\delta^{13}C$ values suggests soil development and maturation in the lake catchment between 15.20 ± 0.26 and 14.05 ± 0.09 cal ka BP.

The relative lake-level in the Wykeham basin lowered between 14.05 ± 0.09 and 13.79 ± 0.08 cal ka BP (WU-3), and the littoral charophyte meadows at the sampling site were replaced by stands of shallow aquatic flora including *Potamogeton pusillus, P. filiformis* and *Myriophyllum spicatum* in waters no deeper than 1.5 m (Table 4). High siliclastic content in WU-3 indicates enhanced allogenic inwash into the palaeolake and destabilised catchment soils occupied by montane herbs (including *S. acaulis* and *A. maritima*). Turnovers in palynological and macrofossil assemblages (e.g. Mortensen et al., 2011; Candy et al., 2016), coversand deposition (e.g. Hoek and Bohncke, 2002) and glacial re-advances (e.g. Mangerud et al., 2016; 2017) in Northern Europe and Scandinavia all occurred in phase with the VoP hydroclimatic shifts in WU-3, and are consistent with colder and regionally more arid

615 hydroclimates in these regions during the Older Dryas chronozone (between *ca* 14.1 and 13.9
616 cal ka BP). These changes occurred in phase with GI-1d in the Greenland ice cores, where a
617 depletion in $\delta^{18}O$ and elevated Ca^{2+} show a climatic deterioration in the high latitudes coupled
618 with regional-to-hemispherical-scale changes in atmospheric circulation (Rasmussen et al.,
619 2014).

620 Charophyte meadows recolonised the marginal sectors of the water body, as effective
621 precipitation recharging the VoP aquifer drove a rise in the groundwater level to optimum
622 interstadial elevations by 13.79 $\pm$ 0.08 cal ka BP. The relative lake-level remained high and
623 the sedimentation rate in the basin declined as accommodation space decreased and stable
624 soils occupied by shrubby taxa developed in the catchment between 13.79 ± 0.08 and 13.45
625 ± 0.08 cal ka BP. *Juniperus communis* needles at the base of WU-4, represents the
626 development of Juniper scrub in the catchment. The timing of *Juniperus* influx into the
627 Wykeham basin is consistent with the first presence of *Juniperus* macrofossils in other records
628 at Wykeham Quarry (Lincoln et al., 2017), as well as a rise in *Juniperus* pollen at Gransmoor
629 (Walker et al., 1993), suggesting a regional expansion of *Juniperus* expansion in the lowlands
630 of NE England between *ca* 14.00 - 13.70 cal ka BP. This is significant, as rises in *Juniperus*
631 have been widely reported from the palynological records of NE England and assumed to
632 reflect direct landscape responses to the rapid warming at the onset of the Lateglacial
633 Interstadial (e.g. Tweddle, 2001). The macrofossil record from Wykeham Quarry and pollen
634 records from Gransmoor, however, demonstrate that the development of *Juniperus* scrub in
635 NE England occurred significantly later than the initial climatic amelioration at the start of the
636 Lateglacial Interstadial, during or soon after the WU-3 hydroclimatic event. Therefore, it is
637 more likely that the expansion of *Juniperus* was driven by increased habitat availability during
638 and/ or soon after the hydroclimatic changes of WU-3 (Day, 1996; Abrook et al., 2017).

639 Palynological records from the VoP (Day, 1996; Abrook, 2017) and Gransmoor (Walker et al.,
640 1993) show that rises in *Betula* pollen to optimum values, after the initial peak in *Juniperus*, is
641 thought to represent the onset of peak Interstadial woodland cover in the region, and therefore
642 highest landscape stability around *ca* 13.8 ka BP (Matthews et al., 2017). Decreases in the
643 sedimentation rate (Figure 3) and depletion in $\delta^{13}C$ values at Wykeham support a stabilisation
644 of the landscape during this interval (section 5.3.2). There is no evidence however for the
645 development of extensive tree cover in the vicinity of the Wykeham basin (section 5.2).

646 At 13.46 ± 0.08 cal ka BP, temperatures declined in the VoP and the groundwater lowered,
647 forming a fen peatland in the basin (WU-5). This occurred in phase with $\delta^{18}O$ and C-IT declines
648 in other British (Brooks and Birks, 2001; Marshall *et al.,* 2002; Candy *et al.,* 2016), and
649 European records (e.g. Heiri et al., 2007; Lotter et al., 2012) suggesting a regional climatic

deterioration equivalent with GI-1b in Greenland and the Gerzensee oscillation in Europe. A shallow lake reformed at Wykeham by 13.08 ± 0.10 cal ka BP (WU-6a), but air temperatures remained low, with vegetation cover declining as open ground herbs replaced shrubby taxa in the lake catchment and allogenic material from unstable soils were washed into the lake basin. This phase is broadly concomitant with a short interval of $\delta^{18}O$ enrichment in the Greenland ice cores (GI-1a) indicative of a temporary amelioration in temperatures (Rasmussen et al., 2014). No substantial enrichment is recorded at Wykeham, suggesting that temperatures in the VoP did not substantially warm during the GI-1a chronozone.

Northern Hemispheric cooling at the start of the GS-1 chronozone reduced carbonate precipitation in the Wykeham basin. Standing water persisted at least seasonally between 12.72 ± 0.06 cal ka BP and 12.29 ± 0.10 cal ka BP (WU-6b), but biogenic productivity within the water column and the catchment was low, with vegetation cover consisting almost entirely of perennial herbs with arctic and/or montane ecological niches. Involuted interstadial deposits elsewhere at Wykeham Quarry show that perennially frozen ground developed under low mean annual temperatures during this interval (Lincoln et al., 2017). In NW Europe, continuous permafrost formed across the northern British Isles and Scandinavia, and it is possible that this maintained perched groundwater bodies across these regions during the initial stages of the Younger Dryas.

The VoP groundwater lowered to below the infill elevation of the Wykeham palaeolake at 12.29 ± 0.10 cal ka BP cal ka BP, promoting the influx of sand and gravel beds from the basin perimeter onto the Wykeham lake bench, and forming hiatuses in the lacustrine records at neighbouring Palaeolake Flixton (Palmer et al., 2015). Any standing water was ephemeral and fed from nival melt and fluvial discharges which temporarily formed a shallow water body within the basin during spring-summer months. It is unclear whether the lower lake-levels were associated with a concomitant shift in temperature, but the low organic content of the sediments, coupled with the absence of any thermophilic macrofossil taxa, suggests that catchment vegetation cover and temperatures remained low. The timing of this hydrological change is poorly resolved at Wykeham (Figure 3), occurring slightly prior to climatic/hydroclimatic shifts during the mid-Younger Dryas elsewhere in Northern Europe (Bakke et al., 2009; Lane et al., 2013) including temporary rises in air temperature in southern Germany (von Grafenstein et al., 1999) and France (Genty et al., 2006) at *ca* 12.15 cal ka BP. It is possible that a temporary rise in temperatures caused perennially frozen ground in the VoP to melt, enabling any standing water in the Wykeham basin to freely drain through the glaciofluvial substrata, but without further chronological control and palaeoclimatic data from the VoP, it is not possible to confidently assign this hydrological signal to the mid-YD transition.

Gravel inwash into the basin ceased at *ca* 11.95 cal ka BP, and the groundwater elevation had risen sufficiently in the VoP to reform a shallow water body in the Wykeham depression. Although no temperature evidence is available from Wykeham, the timing of the lake level rise can be compared to climatic records from neighbouring Palaeolake Flixton (Blockley et al., 2018), where a sharp $\delta^{18}O$ increase occurs within age error of the rise in the Wykeham lake level (Figure 8). This evidence supports the interpretation that a rise in groundwater elevation through the VoP basin occurred during the latter stages of the Younger Dryas/ GS-1 chronozone, prior to the hemispheric amelioration in regional temperatures at the start of the Holocene (*ca* 11.65 cal ka BP). It should be noted that whilst temperatures had begun to ameliorate, the landscape remained open and unstable, with only perennial herbs colonising the catchment.

Two abrupt climatic events (ACE-1 and ACE-2) have been recorded in the Early Holocene records at Palaeolake Flixton (Figure 8) which impacted air temperatures, and ecosystems in the VoP (Blockley et al., 2018). ACE-1 occurred within age uncertainty of the infilling of the lake and the development of fen peat in the Wykeham depression at 11.50 ± 0.13 cal ka BP (WU-8). This event is broadly contemporaneous with the 11.4 ka event in the Greenland ice cores (Rasmussen et al., 2014). It is likely that the climatic deterioration recorded in Palaeolake Flixton promoted a temporary reduction in the groundwater elevation during an interval of lower effective precipitation regimes (e.g. Magny et al., 2007), causing the rapid infill/ hydroseral succession of the Wykeham lake. ACE-2 occurred after the lake had infilled, meaning that no supporting evidence for hydroclimatic changes associated with this climatic oscillation are available from the Wykeham basin.

6. Regional heterogeneity in hydroclimate

The Wykeham basin record demonstrates that hydrological changes accompanied abrupt climatic events during the LGIT but did not always occur in phase with Greenlandic temperature variations. This is notable in the initial amelioration signals (formation of the Wykeham basin, precipitation of authigenic carbonates, and rising $\delta^{18}O$ values) at the base of the Wykeham basin sequence (WU-1 to 2a), which suggests that the VoP was becoming warmer and wetter prior to the abrupt amelioration in Greenland at the start of GI-1e (Figure 8). These reconstructions are in agreement with a series of other European palaeoclimatic records which indicate warming prior to the start of GI-1e (e.g. Walker et al., 2003; Watson et al., 2010; Shakun et al., 2012; Wohlfarth et al., 2018), although in most instances, these archives have less secure chronologies than the Wykeham sequence, limiting secure regional correlations. Furthermore, hydroclimatic changes (rising lake levels) also appear to have been initiated in the VoP, *ca* 0.3 ka prior to the onset of the Holocene at *ca* 11.65 cal ka BP.

Together, these signals support a repeated regional asynchrony in hydroclimatic responses to the two major warming intervals of the LGIT.

During the centennial scale climatic oscillations of the LGIT (~GI-1d and ~GI-1b), lower lake-levels persisted in the Wykeham basin, indicating low effective precipitation regimes recharging the VoP groundwater aquifer under arid hydroclimates. In Northern Europe, in regions between 50-60 ºN, low lake-levels (e.g. Bos et al., 2006) and high evapotranspiration signals (e.g. Rach et al., 2014; 2017; Muschitiello et al., 2015) have been recorded during these climatic oscillations, indicating transitions to more arid conditions in response to abrupt cooling events (section 5.5; Figure 8). Together, these trends show that cooler conditions during the Lateglacial Interstadial (~GI-1d and ~GI-1b), coincided with more arid conditions across abrupt (sub-centennial) transitions in Northern Europe.

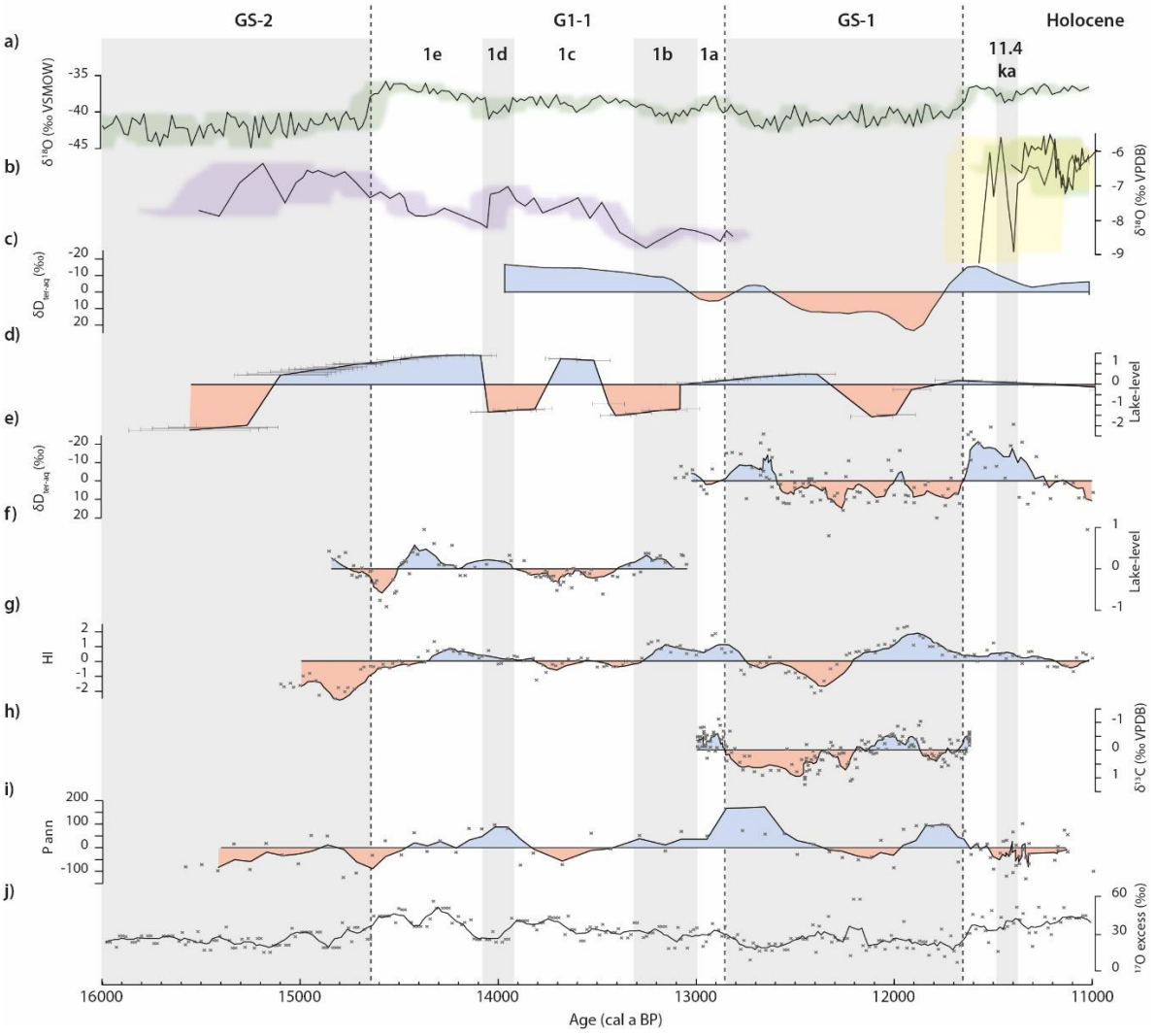

Figure 8. Comparisons of European hydroclimatic records from the North Atlantic seaboard. a) $\delta^{18}O$ from NGRIP is derived from Rasmussen et al. (2006; 2014); b) $\delta^{18}O$ from the Wykeham basin (purple, this study) and Palaeolake Flixton (yellow and green, Blockley et al., 2018) in the VoP; c) $\delta D_{terr\text{-}aq}$ from Hasseldala Port, S. Sweden (Muschitiello et al., 2015); d) Relative lake-level reconstructions from the Wyekham basin (this study); e) $\delta D_{terr\text{-}aq}$ from Meerfelder Maar, Germany (Rach et al., 2014); f) respectively); Relative lake-level reconstructions from Lake Gerzensee, Switzerland (Magny, 2013); g) a hydrological index from Grotta Savi NE Italy (Belli et al., 2017); h) $\delta^{13}C$ isotopes from Seso Cave speleothems in NE Spain (Bartolome et al., 2015); i) reconstructed annual precipitation from Lake Navamuno, Central Spain (López-Sáez et al., 2020), and j) ^{17}O excess, a proxy for midlatitude moisture source conditions for Greenlandic precipitation (Landais et al., 2018). Hydrological records are presented

as residuals from a linear smooth line (section 3.3; Figure 6) with positive residuals (blue) indicating humid signals, and negative residuals (red) indicating arid signals. The Meerfelder Maar, Lake Gerzensee, Grotta Savi, Navamuno and NGRIP ^{17}O excess records are displayed as 5 point moving averages with raw data presented as grey crosses. Grey bands represent cooling events in the Greenland ice cores (i.e. GS-2, GI-1d, GI-1b, GS-1, 11.4 ka event). The locations of these records relative to the VoP are shown in Figure 9.

Central-Southern European records (between 50-40 ºN) show a different response, with higher relative lake-levels (e.g. Magny, 2013) and more humid hydroclimates (e.g. Belli et al., 2017; López-Sáez et al., 2020; Figure 9) persisting through the climatic oscillations during the Lateglacial Interstadial (~GI-1d and ~GI-1b). Hydrological trends through the Younger Dryas chronozone (~GI-1a to GS-1) show shifts to more arid hydroclimates across the European continent (Figure 9), but within this interval, there is additional complexity. The VoP and Northern European records are bi-partitioned into an early humid (high lake-level) phase, followed by a more arid (lower lake-level) phase (Magny and Ruffadi, 1995; Walker, 1995; Diefendorf et al., 2006; Bos et al., 2006). Further south in the Alps and the Iberian Peninsula, more humid conditions/ higher lake-levels were initiated during the late Younger Dryas (< 12.5-12.15 ka BP; e.g. Bartolome et al., 2015; Rossi et al., 2018), prior to Northern Europe. Together these trends demonstrate that hydrological variations are more regionally dynamic than changes in temperature through the LGIT, and that hydrological responses to different cooling phases were manifested differently across the European continent, not necessarily occurring in phase with changes in temperature (Rach et al., 2014).

In the present day, hydroclimatic conditions in the British Isles and NW Europe are largely a function of the position of atmospheric circulation patterns across the North Atlantic Ocean. Interannual to centennial-scale variability in these circulation patterns are manifested through the North Atlantic Oscillation (NAO), but variability in the contemporary modes of the NAO are unlikely to account for the hydroclimatic bifurcations observed through the LGIT for two reasons: (1) model simulations have demonstrated that the pattern of atmospheric circulation varied significantly from contemporary modes, largely due to differences in the initial boundary conditions (e.g. the thickness and extent of Northern Hemispheric ice sheets, greenhouse gas concentrations, sea level pressure, sea-ice extent etc.; e.g. Pausata et al., 2011; Löfverström and Lora, 2017); (2) records of aeolian activity through the LGIT suggest that during cooling intervals, stationary circulation regimes dominated by strong and zonal westerly winds devoid of moisture persisted across the European continent (e.g. Brauer et al., 2008; Costas et al., 2016), which is counter to the current interannual modes of the NAO. Therefore, it is likely that mechanisms other than NAO variability are required to explain the bifurcating hydroclimatic signals observed through the abrupt cooling events of the LGIT.

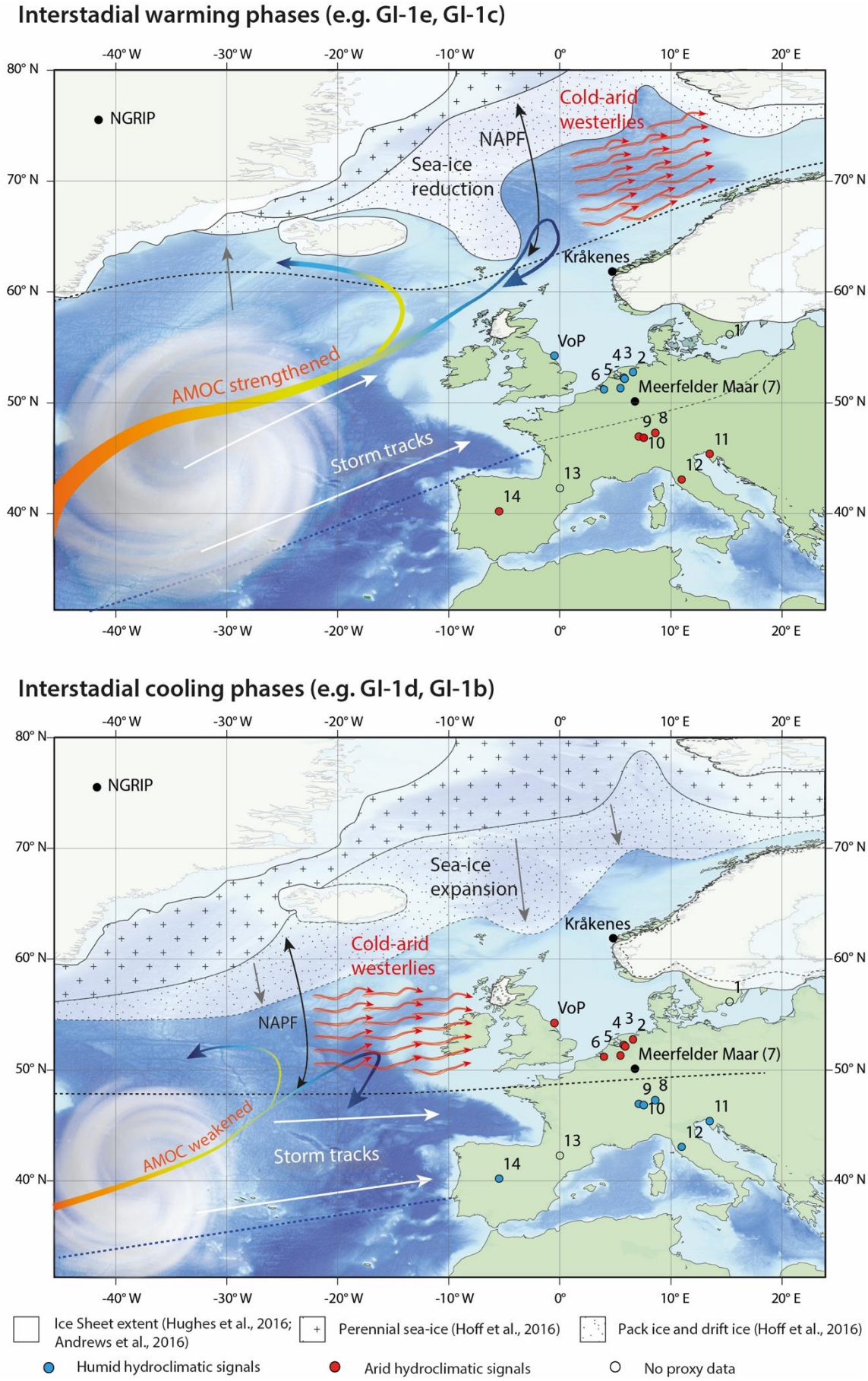
Interstadial warming phases (e.g. GI-1e, GI-1c)
-40° W
-30° W
-20° W
-10° W
0°
10° E
20° E
80° N
70° N
60° N
50° N
40° N
NGRIP
Cold-arid westerlies
NAPF
Sea-ice reduction
Kråkenes
VoP
Meerfelder Maar (7)
AMOC strengthened
Storm tracks
1
2
3
4
5
6
7
8
9
10
11
12
13
14
Interstadial cooling phases (e.g. GI-1d, GI-1b)
Sea-ice expansion
Cold-arid westerlies
NAPF
AMOC weakened
Storm tracks
Ice Sheet extent (Hughes et al., 2016; Andrews et al., 2016)
Perennial sea-ice (Hoff et al., 2016)
Pack ice and drift ice (Hoff et al., 2016)
Humid hydroclimatic signals
Arid hydroclimatic signals
No proxy data

775

Figure 9. Conceptual model illustrating the factors (latitude of sea-ice, NAPF, storm tracks and AMOC strength) responsible for bifurcating hydroclimatic signals during the cooling (GI-1d, GI-1b) and warming intervals (GI-1e, GI-1c) of the Lateglacial Interstadial (GI-1). Details of other hydrological records (1 to 14) displayed as either blue (humid), red (arid), or black (no proxy data) circles are listed in Appendix D. Hydrological proxy data from Hasseldala Port (1; Muschitiello et al., 2015; Wohlfarth et al., 2017), Meerfelder Maar (7; Rach et al., 2014), Lake Gerzensee (10; Magny, 2013), Grotta Savi (11; Belli et al., 2017), Grotta Seso (Bartolome et al., 2015), and Lake Navamuno (López-Sáez et al., 2020) are shown in Figure 8. The sites of Meerfelder Maar and Kråkenes, used as key locations to explain hydroclimatic variability during GS-1 (e.g. Bakke et al., 2009; Lane et al., 2013) are also shown. The extent of the Fennoscandian and British-Irish Ice sheet extents follow Hughes et al. (2016), Greenland and Iceland ice sheet extents follow Andrews et al. (2016), and estimations of sea-ice extent in the North Atlantic follows Hoff et al. (2016). The position of the NAPF, storm tracks, and cold westerly air masses follows the relative hydrological proxy signals from the records, and descriptions by Brauer et al. (2008); Naughton et al. (2019).

Climatic oscillations during the LGIT (GI-1d, GI-1b, GS-1) are most readily attributed to fluctuations in the Atlantic Meridional Overturning Circulation (AMOC) strength via freshwater hosing from the deglaciating Northern Hemispheric ice sheets, disrupting the transfer of latent heat to the continental margins (Broecker and Denton, 1989; Broecker *et al.,* 1990). Changes in regional hydrology associated with these events are attributed to the displacement of moisture bearing westerly winds across the European continent (e.g. Magny et al., 2007; Bakke et al., 2009), and should therefore most strongly affect the hydroclimates of western Europe.

Hydrological bifurcations between Northern and Southern Europe through the climatic oscillations of the LGIT occurred in association with changes in ^{17}O-excess in the Greenland ice cores (Figure 8), interpreted as a proxy for the reorganization of climatic conditions and/or water cycle at latitudes south of Greenland (Guillevic et al., 2014; Landais et al., 2018). It is therefore presumed that the European hydroclimate was sensitive to perturbations in the mid-latitude water cycle, which would have been driven, at least in part, by shifts in the strength and latitude of the jet stream and precipitation-bearing westerly winds across the continent (e.g. Bakke et al., 2009; Lane et al., 2013; Rach et al., 2014), which are themselves sensitive to the latitude of North Atlantic winter sea-ice cover (Isarin et al., 1998; Renssen and Isarin, 2001; Sadatzki et al., 2019; Figure 9).

The position of the North Atlantic Polar Front (NAPF), is a key constituent of hydroclimatic conditions in western Europe (Ruddiman and McIntyre, 1981). Collectively, the regional comparisons discussed above support an interpretation that during the abrupt climatic events of the LGIT, winter sea-ice expansion in the North Atlantic initiated a southerly migration of the NAPF (e.g. Denton et al., 2005; Renssen et al., 2018; Muschitiello et al., 2019; Naughton et al., 2019), the focussing of stronger and more zonal westerly winds devoid of moisture across Northern Europe (Brauer et al., 2008), and the depression of moisture bearing subpolar cyclonic activity into Central and Southern Europe (e.g. Marchal et al., 2016; Pauly et al., 2018). This caused increased aridity between *ca* 50 to 60 ºN (e.g. Hoek and Bohncke, 2002; Bos et al., 2006) and increased humidity between *ca* 40 to 50 ºN (Magny, 2001; Belli et al., 2017). Regional hydrological bifurcations similar to those observed during the climatic oscillations of the Lateglacial Interstadial have been reconstructed during the Early Holocene

(e.g. the 11.4 ka event and the 8.2 ka event; Magny et al., 2003; 2007), suggesting that this is a consistent response to abrupt cooling events during both glacial and interglacial climatic regimes across the European continent.

Changes in hydroclimatic signals through GS-1 (including the Younger Dryas in Europe) are more complex than those in GI-1d and GI-1b, and have also been attributed to the position of the NAPF across the European continent (e.g. Brauer et al., 2008; Bakke et al., 2009; Lane et al., 2013; Rach et al., 2014; Naughton et al., 2019). The findings presented here broadly supports these interpretations (i.e. enhanced Northern European aridity associated with cooling; Figure 8), but also highlight that this model is too simplistic, and cannot explain the internal hydroclimatic structure and leads and lags associated with the onset of GS-1. This is most notable during the initial stages of GS-1 (i.e. *ca* 12.90 to 12.70 cal ka BP), where more humid conditions in Northern European records persist for *ca* 0.17 ka after the onset of GS-1, before switching to arid hydroclimatic signals at the start of the Younger Dryas at *ca* 12.68 cal ka BP (e.g. Rach et al., 2014; Muschitiello et al., 2015). At Wykeham, relatively humid conditions persisted for at least 0.17 ka after the start of GS-1, before transitioning to a more arid signal. This observation indicates that the shifts to colder conditions during GS-1 did not immediately lead to more arid hydroclimates in Northern Europe. In contrast, the Lateglacial Interstadial events in Northern Europe, cooling is associated with what appears to be an immediate change to increased aridity, a change that is also detected within chronological uncertainties to temperature ($\delta^{18}O$) changes in the Greenland ice cores (Rasmussen et al., 2014).

One explanation for the lag in hydrological response during GS-1 has been attributed to the time taken for the southerly displacement and stabilisation of the NAPF and sea-ice edge in the North Atlantic Ocean in response to reduced AMOC strength (Rach et al., 2014). It should also be noted that the hydrological lag in Europe to cooling at the start of GS-1 is longer than the entire duration of GI-1d in the Greenland ice cores (*ca* 0.12 ka), which suggests that the hydrological and environmental responses to the abrupt cooling episodes of the Lateglacial Interstadial (GI-1b and GI-1d) were more closely synchronised with regional cooling than at the onset of the GS-1/YD period. Whilst there may be some limitations to these comparisons on the basis of chronological resolution, it is clear that hydroclimatic changes associated with abrupt climatic changes in Europe were dynamic, and cannot be assumed to occur concurrently with either: a) $\delta^{18}O$ changes in the Greenland ice cores (e.g. Bakke et al., 2009; Rach et al., 2014; Muschitiello et al., 2015); or b) hydrological changes occurring across the rest of the European continent. Further high-resolution records, coupled with robust chronologies are therefore required, particularly during intervals of abrupt changes in

852 temperature, to further investigate the spatiotemporal differences and more precisely
853 constrain the hydroclimatic leads and lags associated with these events.

854 ## 7. Conclusions

855 The palaeolake basin at Wykeham Quarry provides the only currently available high-
856 resolution, chronologically constrained account of hydroclimatic changes, coupled with
857 changes in local environmental conditions, occurring in the British Isles across the entire LGIT.
858 Several climatic oscillations are identified, which affected catchment vegetation cover and
859 lake-levels, demonstrating a direct link between cooling intervals and phases of enhanced
860 aridity in NE England. During cooling intervals (~GI-1d, ~GI-1b, ~GS-1), the local environment
861 was dominated open ground perennial taxa, which were replaced by shrub-rich flora (e.g.
862 *Empetrum nigrum,* and *Juniperus communis*) during the warmer episodes (~GI-1e, ~GI-1c).
863 Based upon comparisons with the Greenland ice-core event stratigraphy, it is clear that
864 hydrological shifts in the VoP were, in some instances, asynchronous with temperature
865 changes in Greenland. Comparisons to hydrological records elsewhere in Europe show a
866 latitudinal bifurcation, with Northern European records becoming more arid, and southern
867 records becoming more humid in response to climatic events during the Lateglacial
868 Interstadial (GI-1d and GI-1b). Hydroclimatic signals in GS-1 are more complex, with Northern
869 Europe initially becoming more humid before a secondary phase of enhanced aridity. In
870 Central and Southern European records, the opposite trend is seen, with enhanced aridity
871 transitioning to more humid hydroclimates. Shifting positions of the polar front across the North
872 Atlantic seaboard in response to AMOC strength, and the position of the sea-ice margin, is
873 thought to explain this phenomenon. The additional complexity within GS-1 however is not
874 readily explained using these criteria, and further records are required to test these
875 hypotheses. While the evidence for dynamic shifts in hydroclimate exist across Europe, these
876 interpretations are based on a limited number of locations and a variety of methods. Additional
877 high-resolution hydroclimatic records coupled with robust chronologies are required in order
878 to further investigate hydroclimatic leads and lags, and patterns of spatiotemporal differences
879 associated with intervals of abrupt climatic change through the LGIT.

880 ## Acknowledgements

881 This work was undertaken as part of PCL's PhD research, funded by Hanson Aggregates.
882 PCL gratefully acknowledges Robert Pigg for access to the land, and to Stuart Laws and Tim
883 Harvey from Hanson Aggregates for access, advice, and assistance whilst working at
884 Wykeham Quarry. The authors also extend thanks to Ashley Abrook, Rhys Timms, and the
885 MSc Quaternary Science cohort of 2014-2015 for assistance in the field, and to David Lowry

for the use of the stable isotope laboratory in the Department of Earth Sciences at Royal Holloway.

References

Abrook, A., 2017. Vegetation changes at Palaeolake Flixton during the Late-glacial and Early Holocene periods. In: Lincoln, P.C. Eddey, L.J., Matthews, I.P., Palmer, A.P. and Bateman, M.D. (eds.). 2017. The Quaternary of the Vale of Pickering: Field Guide. Quaternary Research Association, London.

Ashley, G.M., 1975. Rhythmic sedimentation in glacial lake Hitchcock, Massachusetts, Connecticut. In: Jopling, A.V., McDonald, B.C. (Eds.). Glaciofluvial and Glaciolacustrine Sedimentation. Society of Economic Palaeontologists and Mineralogists, Special Publication No. 23, pp. 304-320.

Atkinson, T. C., Briffa, K. R., and Coope, G. R. 1987. Seasonal temperatures in Britain during the past 22,000 years, reconstructed using beetle remains. *Nature*, *325*, 587-592.

Bakke, J., Lie, Ø., Heegaard, E., Dokken, T., Haug, G.H., Birks, H.H., Dulski, P. and Nilsen, T., 2009. Rapid oceanic and atmospheric changes during the Younger Dryas cold period. *Nature Geoscience*, *2*(3), pp.202-205.

Bartolomé, M., Moreno, A., Sancho, C., Stoll, H.M., Cacho, I., Spötl, C., Belmonte, Á., Edwards, R.L., Cheng, H. and Hellstrom, J.C., 2015. Hydrological change in Southern Europe responding to increasing North Atlantic overturning during Greenland Stadial 1. *Proceedings of the National Academy of Sciences*, *112*(21), pp.6568-6572.

Batchelor, C.R. 2009. Northern Extension and Southern Extensions, Wykeham Quarry: Geoarchaeological Deposit Models, Interim Report. Quaternary Scientific Unpublished Report

Battarbee, R.W., 2000. Palaeolimnological approaches to climate change, with special regard to the biological record. *Quaternary Science Reviews*, *19*(1-5), pp.107-124.

Belli, R., Borsato, A., Frisia, S., Drysdale, R., Maas, R. and Greig, A., 2017. Investigating the hydrological significance of stalagmite geochemistry (Mg, Sr) using Sr isotope and particulate element records across the Late Glacial-to-Holocene transition. *Geochimica et Cosmochimica Acta*, *199*, pp.247-263.

Bennike, O., 1998. Fossil egg sacs of Diaptomus (Crustaceae: Copepoda) in Late Quaternary lake sediments. *Journal of Paleolimnology*, *19*(1), pp.77-79.

Berggren, G., 1964. Atlas of Seeds. Part 2. Cyperaceae. Swedish Natural Science Research

Birks, H. H., 1980. Plant macrofossils in Quaternary lake sediments. Archiv fur Hydrobiologie Beiheft, 15: 1–60.

Birks, H.H., 2002. Plant macrofossils. In *Tracking environmental change using lake sediments* (pp. 49-74). Springer Netherlands.

Birks, H.H. and Birks, H.J.B., 2014. To what extent did changes in July temperature influence Lateglacial vegetation patterns in NW Europe? Quaternary Science Reviews, 106, pp.262-277.

Birks, H.H. and Mathewes, R.W., 1978. Studies in the vegetational history of Scotland. *New Phytologist*, *80*(2), pp.455-484.

Blockley, S.P., Lowe, J.J., Walker, M.J., Asioli, A., Trincardi, F., Coope, G.R. and Donahue, R.E., 2004. Bayesian analysis of radiocarbon chronologies: examples from the European Late-glacial. *Journal of Quaternary Science*, *19*(2), pp.159-175.

Blockley, S., Candy, I., Matthews, I., Langdon, P., Langdon, C., Palmer, A., Lincoln, P.C., Abrook, A., Taylor, B., Conneller, C. and Bayliss, A., 2018. The resilience of postglacial hunter-gatherers to abrupt climate change. *Nature ecology & evolution*, *2*(5), p.810.

Bohncke, S. and Wijmstra, L., 1988. Reconstruction of Late-Glacial lake-level fluctuations in The Netherlands based on palaeobotanical analyses, geochemical results and pollen-density data. *Boreas*, 17(3), pp.403-425

Bos, J.A., Bohncke, S.J. and Janssen, C.R., 2006. Lake-level fluctuations and small-scale vegetation patterns during the late glacial in The Netherlands. *Journal of Paleolimnology*, *35*(2), pp.211-238.

Boston, C.M., Lukas, S. and Carr, S.J., 2015. A Younger Dryas plateau icefield in the Monadhliath, Scotland, and implications for regional palaeoclimate. *Quaternary Science Reviews*, 108, pp.139-162.

Brauer, A., Haug, G.H., Dulski, P., Sigman, D.M. and Negendank, J.F., 2008. An abrupt wind shift in western Europe at the onset of the Younger Dryas cold period. *Nature Geoscience*, *1*(8), pp.520-523.

Brock, F., Higham, T., Ditchfield, P. and Bronk Ramsey, C., 2010. Current pretreatment methods for AMS radiocarbon dating at the Oxford Radiocarbon Accelerator Unit (ORAU). *Radiocarbon*, *52*(1), pp.103-12.

Broecker, W.S. and Denton, G.H., 1989. The role of ocean-atmosphere reorganizations in glacial cycles. *Geochimica et Cosmochimica Acta*, *53*(10), pp.2465-2501.

Broecker, W.S., Bond, G., Klas, M., Bonani, G. and Wolfli, W., 1990. A salt oscillator in the glacial Atlantic? 1. The concept. *Paleoceanography*, *5*(4), pp.469-477.

Bronk Ramsey, C. (2008). Deposition models for chronological records. *Quaternary Science Reviews, 27*(1-2), 42-60.

Bronk Ramsey, C. (2009). Dealing with outliers and offsets in radiocarbon dating. *Radiocarbon, 51*(3), 1023-1045.

Bronk Ramsey, C., and Lee, S. (2013). Recent and Planned Developments of the Program OxCal. *Radiocarbon, 55*(2-3), 720-730.

Brooks, S.J. and Birks, H.J.B., 2000. Chironomid-inferred Late-glacial air temperatures at Whitrig Bog, Southeast Scotland. *Journal of Quaternary Science*, *15*(8), pp.759-764.

950 Brooks, S.J., Matthews, I.P., Birks, H.H. and Birks, H.J.B., 2012. High resolution Lateglacial and early-
951 Holocene summer air temperature records from Scotland inferred from chironomid assemblages. *Quaternary*
952 *Science Reviews*, *41*, pp.67-82.

953 Brown, T., Bradley, C., Grapes, T. and Boomer, I., 2011. Hydrological assessment of Star Carr and the
954 Hertford catchment, Yorkshire, UK. *Journal of Wetland Archaeology*, *11*(1), pp.36-55.

955 Buizert, C., Gkinis, V., Severinghaus, J.P., He, F., Lecavalier, B.S., Kindler, P., Leuenberger, M., Carlson,
956 A.E., Vinther, B., Masson-Delmotte, V. and White, J.W., 2014. Greenland temperature response to climate
957 forcing during the last deglaciation. *Science*, *345*(6201), pp.1177-1180.

958 Bullock, P., Fedoroff, N., Jongerius, A., Stoops, G., Tursina, T. 1985. *Handbook for soil thin section description*,
959 Waine Research, Chicago.

960 Candy, I., Farry, A., Darvill, C. M., Palmer, A., Blockley, S. P. E., Matthews, I. P., MacLeod, A., Deeprose, L.,
961 Farley, N., Kearney, R., Conneller, C., Taylor, B., and Milner, N., 2015. The evolution of Palaeolake Flixton
962 and the environmental context of Star Carr: an oxygen and carbon isotopic record of environmental change
963 for the early Holocene. *Proceedings of the Geologists' Association*, *126*(1), 60-71.

964 Candy, I., Abrook, A., Elliot, F., Lincoln, P., Matthews, I.P. and Palmer, A., 2016. Oxygen isotopic evidence for
965 high-magnitude, abrupt climatic events during the Lateglacial Interstadial in north-west Europe: analysis of a
966 lacustrine sequence from the site of Tirinie, Scottish Highlands. *Journal of Quaternary Science*, *31*(6), pp.607-
967 621.

968 Candy, I., Palmer, A.P., Blockley, S.P.E., Matthews, I.P., MacLeod, A., Farley, N., Farry, A., Kearney, R.,
969 Abrook, A., Darvill., C. $\delta^{13}C$ and $\delta^{18}O$ analysis of lacustrince marls from Palaeolake Flixton. In: Lincoln, P.C.
970 Eddey, L.J., Matthews, I.P., Palmer, A.P. and Bateman, M.D. (eds.). 2017. The Quaternary of the Vale of
971 Pickering: Field Guide. Quaternary Research Association, London.

972 Cappers, R.T., René, T.J., Becker, R.M. and Jans, J.E., 2006. *Digital seed atlas of the Netherlands. Groningen*
973 *Archaeological Studies, Volume 4*. Barkhuis Publishing and Groningen University Library, Groningen, 502pp.
974 (in Dutch). Clark et al., 2001

975 Carey, M.A. and Chadha, D., 1998. Modelling the hydraulic relationship between the River Derwent and the
976 Corallian Limestone aquifer. *Quarterly Journal of Engineering Geology and Hydrogeology*, *31*(1), pp.63-72.

977 Chandler, B.M., Boston, C.M. and Lukas, S., 2019. A spatially-restricted Younger Dryas plateau icefield in the
978 Gaick, Scotland: Reconstruction and palaeoclimatic implications. *Quaternary Science Reviews*, 211, pp.107-
979 135.

980 Clark, P.U., Pisias, N.G., Stocker, T.F. and Weaver, A.J., 2002. The role of the thermohaline circulation in
981 abrupt climate change. *Nature*, *415*(6874), pp.863-869.

982 Cohen, A.S., 2003. *Paleolimnology: the history and evolution of lake systems*. Oxford University Press.

983 Costas, S., Naughton, F., Goble, R. and Renssen, H., 2016. Windiness spells in SW Europe since the last
984 glacial maximum. *Earth and Planetary Science Letters*, *436*, pp.82-92.

Darling, W. G. 2004. Hydrological factors in the interpretation of stable isotopic proxy data present and past: a European perspective. *Quaternary Science Reviews*, 23 (7), 743-770.

Darling, W.G., and Talbot, J.C., 2003. The O and H stable isotopic composition of fresh waters in the British Isles: 1. *Rainfall, Hydrology and Earth System Sciences*, 7, 163–181.

Day, P., 1996. Devensian Late-glacial and early Flandrian environmental history of the Vale of Pickering, Yorkshire, England*. Journal of Quaternary Science,* 11, 9-24.

Dean, W.E., 1974. Determination of carbonate and organic matter in calcareous sediments and sedimentary rocks by loss on ignition: comparison with other methods. *Journal of Sedimentary Research*, *44*(1).

Denton, G.H., Alley, R.B., Comer, G.C. and Broecker, W.S., 2005. The role of seasonality in abrupt climate change. *Quaternary Science Reviews*, *24*(10), pp.1159-1182.

Diefendorf, A.F., Patterson, W.P., Mullins, H.T., Tibert, N. and Martini, A., 2006. Evidence for high-frequency late Glacial to mid-Holocene (16,800 to 5500 cal yr BP) climate variability from oxygen isotope values of Lough Inchiquin, Ireland. *Quaternary Research*, *65*(1), pp.78-86.

Dieffenbacher-Krall, A. and Halteman, W., 2000. The relationship of modern plant remains to water depth in alkaline lakes in New England, USAe. *Journal of Paleolimnology*, *24*(2), pp.213-229.

Drummond, C.N., Patterson, W.P. and Walker, J.C., 1995. Climatic forcing of carbon-oxygen isotopic covariance in temperate-region marl lakes. *Geology*, 23(11), pp.1031-1034.

Elias, S. A., and Matthews, I. P. 2013. A comparison of reconstructions based on aquatic and terrestrial beetle assemblages: Late glacial–Early Holocene temperature reconstructions for the British Isles. *Quaternary International*, *341*, 69-79.

Evans, D.J., Bateman, M.D., Roberts, D.H., Medialdea, A., Hayes, L., Duller, G.A., Fabel, D. and Clark, C.D., 2017. Glacial Lake Pickering: stratigraphy and chronology of a proglacial lake dammed by the North Sea Lobe of the British–Irish Ice Sheet. *Journal of Quaternary Science*. *32* (2). 295-310

Gale, S. J. and Hoare, P. G. 1991 *Quaternary sediments: petrographic methods for the study of unlithified rocks*, Belhaven, London.

Genty, D., Blamart, D., Ghaleb, B., Plagnes, V., Causse, C., Bakalowicz, M., Zouari, K., Chkir, N., Hellstrom, J., Wainer, K. and Bourges, F., 2006. Timing and dynamics of the last deglaciation from European and North African δ13C stalagmite profiles—comparison with Chinese and South Hemisphere stalagmites. *Quaternary Science Reviews*, *25*(17-18), pp.2118-2142.

Guillevic, M., Bazin, L., Landais, A., Stowasser, C., Masson-Delmotte, V., Blunier, T., Eynaud, F., Falourd, S., Michel, E., Minster, B. and Popp, T., 2014. Evidence for a three-phase sequence during Heinrich Stadial 4 using a multiproxy approach based on Greenland ice core records. *Climate of the Past*, *10*(6), pp.2115-2133.

Hammarlund, D., Aravena, R., Barnekow, L., Buchardt, B. and Possnert, G., 1997. Multi-component carbon isotope evidence of early Holocene environmental change and carbon-flow pathways from a hard-water lake in northern Sweden. *Journal of Paleolimnology*, *18*(3), pp.219-233.

Hammarlund, D., Björck, S., Buchardt, B., Israelson, C. and Thomsen C.T., 2003. Rapid hydrological changes during the Holocene revealed by stable isotope records of lacustrine carbonates from Lake Igelsjön, southern Sweden. *Quaternary Science Reviews*, 22, 353–370.

Hannon, G.E. and Gaillard, M.J., 1997. The plant-macrofossil record of past lake-level changes. *Journal of Paleolimnology*, *18*(1), pp.15-28.

Harrison, S.P. and Digerfeldt, G., 1993. European lakes as palaeohydrological and palaeoclimatic indicators. *Quaternary Science Reviews*, *12*(4), pp.233-248.

Heiri, O., Cremer, H., Engels, S., Hoek, W.Z., Peeters, W. and Lotter, A.F., 2007. Lateglacial summer temperatures in the Northwest European lowlands: a chironomid record from Hijkermeer, the Netherlands. *Quaternary Science Reviews*, 26(19), pp.2420-2437.

Heiri, O., Brooks, S.J., Renssen, H., Bedford, A., Hazekamp, M., Ilyashuk, B., Jeffers, E.S., Lang, B., Kirilova, E., Kuiper, S. and Millet, L., 2014. Validation of climate model-inferred regional temperature change for late-glacial Europe. *Nature communications*, *5*, p.4914.

Hoek, W.Z. and Bohncke, S.J.P., 2002. Climatic and environmental events over the Last Termination, as recorded in The Netherlands: a review. *Netherlands Journal of Geosciences/Geologie en Mijnbouw*, *81*(1).

Hoff, U., Rasmussen, T.L., Stein, R., Ezat, M.M. and Fahl, K., 2016. Sea ice and millennial-scale climate variability in the Nordic seas 90 kyr ago to present. *Nature communications*, *7*, p.12247.

Isarin, R.F., Renssen, H. and Vandenberghe, J., 1998. The impact of the North Atlantic Ocean on the Younger Dryas climate in northwestern and central Europe. *Journal of Quaternary Science*, *13*(5), pp.447-453.

Kendall, P.F., 1902. A system of glacier-lakes in the Cleveland Hills. *Quarterly Journal of the Geological Society*, *58*(1-4), pp.471-571.

Landais, A., Capron, E., Masson-Delmotte, V., Toucanne, S., Rhodes, R.H., Popp, T., Vinther, B., Minster, B. and Prié, F., 2018. Ice core evidence for decoupling between midlatitude atmospheric water cycle and Greenland temperature during the last deglaciation. *Climate of the Past*, *14*(10), pp.1405-1415.

Lane, C.S., Brauer, A., Blockley, S.P. and Dulski, P., 2013. Volcanic ash reveals time-transgressive abrupt climate change during the Younger Dryas. *Geology*, *41*(12), pp.1251-1254.

Leng, M. J., and Marshall, J. D. 2004. Palaeoclimate interpretation of stable isotope data from lake sediment archives. *Quaternary Science Reviews*, 23 (7), 811-831.

Lincoln, P.C. Eddey, L.J., Matthews, I.P., Palmer, A.P. and Bateman, M.D. (eds.). 2017. The Quaternary of the Vale of Pickering: Field Guide. Quaternary Research Association, London.

López-Sáez, J.A., Carrasco, R.M., Turu, V., Ruiz-Zapata, B., Gil-García, M.J., Luelmo-Lautenschlaeger, R., Pérez-Díaz, S., Alba-Sánchez, F., Abel-Schaad, D., Ros, X. and Pedraza, J., 2020. Late Glacial-early holocene vegetation and environmental changes in the western Iberian Central System inferred from a key site: The Navamuño record, Béjar range (Spain). *Quaternary Science Reviews*, *230*, p.106-167.

Lotter, A.F., Heiri, O., Brooks, S., van Leeuwen, J.F., Eicher, U. and Ammann, B., 2012. Rapid summer temperature changes during Termination 1a: high-resolution multi-proxy climate reconstructions from Gerzensee (Switzerland). *Quaternary Science Reviews*, 36, pp.103-113.

Löfverström, M. and Lora, J.M., 2017. Abrupt regime shifts in the North Atlantic atmospheric circulation over the last deglaciation. *Geophysical Research Letters*, *44*(15), pp.8047-8055.

Lowe, J.J., Coope, G.R., Sheldrick, C., Harkness, D.D. and Walker, M.J.C., 1995. Direct comparison of UK temperatures and Greenland snow accumulation rates, 15000—12000 yr ago. *Journal of Quaternary Science*, *10*(2), pp.175-180.

Lowe, J.J., Rasmussen, S.O., Björck, S., Hoek, W.Z., Steffensen, J.P., Walker, M.J. and Yu, Z.C., 2008. Synchronisation of palaeoenvironmental events in the North Atlantic region during the Last Termination: a revised protocol recommended by the INTIMATE group. *Quaternary Science Reviews*, *27*(1), pp.6-17.

Lowe, J.J., Matthews, I.P., Mayfield, R., Lincoln, P.C., Palmer, A.P, Staff, R.A. and Timms, R.G.O., 2019. On the timing of retreat of the Loch Lomond ('Younger Dryas') Readvance icefield in the SW Scottish Highlands and its wider significance. *Quaternary Science Reviews*, 219, pp.171-186.

Magny, M. and Ruffadi, P., 1995. Younger Dryas and early Holocene lake-level fluctuations in the Jura mountains, France. *Boreas*, *24*(2), pp.155-172.

Magny, M., Bégeot, C., Guiot, J. and Peyron, O., 2003. Contrasting patterns of hydrological changes in Europe in response to Holocene climate cooling phases. *Quaternary Science Reviews*, 22(15-17), pp.1589-1596.

Magny, M., Vannière, B., De Beaulieu, J.L., Bégeot, C., Heiri, O., Millet, L., Peyron, O. and Walter-Simonnet, A.V., 2007. Early-Holocene climatic oscillations recorded by lake-level fluctuations in west-central Europe and in central Italy. *Quaternary Science Reviews*, *26*(15), pp.1951-1964.

Magny, M., 2013. Climatic and environmental changes reflected by lake-level fluctuations at Gerzensee from 14,850 to 13,050 yrBP. *Palaeogeography, Palaeoclimatology, Palaeoecology*, *391*, pp.33-39.

Mangerud, J., Aarseth, I., Hughes, A.L., Lohne, Ø.S., Skår, K., Sønstegaard, E. and Svendsen, J.I., 2016. A major re-growth of the Scandinavian Ice Sheet in western Norway during Allerød-Younger Dryas. *Quaternary Science Reviews*, 132, pp.175-205.

Mangerud, J., Briner, J.P., Goslar, T. and Svendsen, J.I., 2017. The Bølling-age Blomvåg Beds, western Norway: implications for the Older Dryas glacial re-advance and the age of the deglaciation. *Boreas*, *46*(2), pp.162-184.

Marchal, O., Waelbroeck, C. and Colin de Verdière, A., 2016. On the movements of the North Atlantic subpolar front in the preinstrumental past. *Journal of Climate*, *29*(4), pp.1545-1571

Marshall, J. D., Jones, R. T., Crowley, S. F., Oldfield, F., Nash, S., and Bedford, A. 2002. A high resolution late-glacial isotopic record from Hawes Water, northwest England: Climatic oscillations: Calibration and comparison of palaeotemperature proxies. *Palaeogeography, Palaeoclimatology, Palaeoecology*, *185*(1), 25-40.

Marshall, J. D., Lang, B., Crowley, S. F., Weedon, G. P., van Calsteren, P., Fisher, E. H., Holme, R., Holmes, J.A., Jones, R.T., Bedford, A. and Brooks, S. J. 2007. Terrestrial impact of abrupt changes in the North Atlantic thermohaline circulation: Early Holocene, UK. *Geology*,*35*(7), 639-642.

Matthews, I.P., Abrook, A., Lincoln, P.C. and Palmer, A.P. The Last Glacial Interglacial Transition (16-8 ka BP) in North East England. In: Lincoln, P.C. Eddey, L.J., Matthews, I.P., Palmer, A.P. and Bateman, M.D. (eds.). 2017. The Quaternary of the Vale of Pickering: Field Guide. Quaternary Research Association, London.

Mauquoy D, van Geel B. 2007. Mire and peat macros. In Encyclopedia of Quaternary Science, Vol. 3, Elias SA (ed.). Elsevier: Amsterdam; 2315–2336.

McConnaughey, T., 1991. Calcification in Chara corallina: CO_2 hydroxylation generates protons for bicarbonate assimilation. *Limnology and Oceanography*, *36*(4), pp.619-628.

Mellars, P., and Dark, P., 1998. Star Carr in context: new archaeological and palaeoecolgical investigations at the early Mesolithic site of Star Carr, North Yorkshire. Cambridge: McDonald Institute.

Milner, N., Conneller, C. and Taylor, B., 2018. *Star Carr, Volume 1: a persistent place in a changing world*. White Rose University Press.

Moreno, A., Svensson, A., Brooks, S.J., Connor, S., Engels, S., Fletcher, W., Genty, D., Heiri, O., Labuhn, I., Perşoiu, A. and Peyron, O., 2014. A compilation of Western European terrestrial records 60–8 ka BP: towards an understanding of latitudinal climatic gradients. *Quaternary Science Reviews*, *106*, pp.167-185.

Mortensen, M. F., Birks, H. H., Christensen, C., Holm, J., Noe-Nygaard, N., Odgaard, B. V., Olsen, J. and Rasmussen, K. L. 2011. Lateglacial vegetation development in Denmark–new evidence based on macrofossils and pollen from Slotseng, a small-scale site in southern Jutland. *Quaternary Science Reviews*, *30*(19), 2534-2550.

Murphy, D.H. and Wilkinson, B.H., 1980. Carbonate deposition and facies distribution in a central Michigan marl lake. *Sedimentology*, *27*(2), pp.123-135.

Muschitiello, F., Pausata, F.S., Watson, J.E., Smittenberg, R.H., Salih, A.A., Brooks, S.J., Whitehouse, N.J., Karlatou-Charalampopoulou, A. and Wohlfarth, B., 2015. Fennoscandian freshwater control on Greenland hydroclimate shifts at the onset of the Younger Dryas. *Nature communications*, *6*, 8939.

Muschitiello, F., D'Andrea, W.J., Schmittner, A., Heaton, T.J., Balascio, N.L., DeRoberts, N., Caffee, M.W., Woodruff, T.E., Welten, K.C., Skinner, L.C. and Simon, M.H., 2019. Deep-water circulation changes lead North Atlantic climate during deglaciation. *Nature communications*, *10*(1), p.1272.

Naughton, F., Costas, S., Gomes, S.D., Desprat, S., Rodrigues, T., Goñi, M.S., Renssen, H., Trigo, R., Bronk-Ramsey, C., Oliveira, D. and Salgueiro, E., 2019. Coupled ocean and atmospheric changes during Greenland stadial 1 in southwestern Europe. *Quaternary Science Reviews*, 212, pp.108-120.

Palmer, A. P., Lee, J.A., Kemp, R.A., Carr, S.J. 2008. *Revised laboratory procedures for the preparation of thin sections from unconsolidated material*. Unpublished Internal Report, Royal Holloway, University of London.

Palmer, A.P., Matthews, I.P., Candy, I., Blockley, S.P.E., MacLeod, A., Darvill, C.M., Milner, N., Conneller, C. and Taylor, B., 2015. The evolution of Palaeolake Flixton and the environmental context of Star Carr, NE. Yorkshire: stratigraphy and sedimentology of the Last Glacial-Interglacial Transition (LGIT) lacustrine sequences. *Proceedings of the Geologists' Association*, *126*(1), pp.50-59.

Pauly, M., Helle, G., Miramont, C., Büntgen, U., Treydte, K., Reinig, F., Guibal, F., Sivan, O., Heinrich, I., Riedel, F. and Kromer, B., 2018. Subfossil trees suggest enhanced Mediterranean hydroclimate variability at the onset of the Younger Dryas. *Scientific reports*, 8(1), pp.1-8.

Pausata, F.S.R., Li, C., Wettstein, J.J., Kageyama, M., Nisancioglu, K.H., 2011. The key role of topography in altering North Atlantic atmospheric circulation during the last glacial period. *Climate of the Past*, 7 (4), 1089–1101. doi: 10.5194/cp-7-1089-2011.

Pentecost, A., 2009. The marl lakes of the British Isles. *Freshwater Reviews*, 2(2), pp.167-198.

Rach, O., Brauer, A., Wilkes, H. and Sachse, D., 2014. Delayed hydrological response to Greenland cooling at the onset of the Younger Dryas in western Europe. *Nature Geoscience*, *7*(2), pp.109-112.

Rach, O., Kahmen, A., Brauer, A. and Sachse, D., 2017. A dual-biomarker approach for quantification of changes in relative humidity from sedimentary lipid D/H ratios. *Climate of the Past*, *13*(7), pp.741-757.

Rahmstorf, S., Feulner, G., Mann, M.E., Robinson, A., Rutherford, S. and Schaffernicht, E.J., 2015. Exceptional twentieth-century slowdown in Atlantic Ocean overturning circulation. *Nature climate change*, *5*(5), pp.475-480.

Rasmussen, S.O., Andersen, K.K., Svensson, A.M., Steffensen, J.P., Vinther, B.M., Clausen, H.B., Siggaard-Andersen, M.L., Johnsen, S.J., Larsen, L.B., Dahl-Jensen, D. and Bigler, M., 2006. A new Greenland ice core chronology for the last glacial termination. *Journal of Geophysical Research: Atmospheres*, *111*(D6).

Rasmussen, S.O., Bigler, M., Blockley, S.P., Blunier, T., Buchardt, S.L., Clausen, H.B., Cvijanovic, I., Dahl-Jensen, D., Johnsen, S.J., Fischer, H. and Gkinis, V., 2014. A stratigraphic framework for abrupt climatic changes during the Last Glacial period based on three synchronized Greenland ice-core records: refining and extending the INTIMATE event stratigraphy. *Quaternary Science Reviews*, *106*, pp.14-28.

Reimer, P.J., Bard, E., Bayliss, A., Beck, J.W., Blackwell, P.G., Ramsey, C.B., Buck, C.E., Cheng, H., Edwards, R.L., Friedrich, M. and Grootes, P.M., 2013. IntCal13 and Marine13 radiocarbon age calibration curves 0–50,000 years cal BP. *Radiocarbon*, *55*(4), pp.1869-1887.

Renssen, H. and Isarin, R.F., 2001. The two major warming phases of the last deglaciation at~ 14.7 and~ 11.5 ka cal BP in Europe: climate reconstructions and AGCM experiments. *Global and Planetary Change*, *30*(1), pp.117-153.

Renssen, H., Goosse, H., Roche, D.M. and Seppä, H., 2018. The global hydroclimate response during the Younger Dryas event. *Quaternary Science Reviews*, 193, pp.84-97.

Rossi, C., Bajo, P., Lozano, R.P. and Hellstrom, J., 2018. Younger Dryas to Early Holocene paleoclimate in Cantabria (N Spain): Constraints from speleothem Mg, annual fluorescence banding and stable isotope records. *Quaternary Science Reviews*, *192*, pp.71-85.

Ruddiman, W.F. and McIntyre, A., 1981. The North Atlantic Ocean during the last deglaciation. *Palaeogeography, Palaeoclimatology, Palaeoecology*, *35*, pp.145-214.

Sadatzki, H., Dokken, T.M., Berben, S.M., Muschitiello, F., Stein, R., Fahl, K., Menviel, L., Timmermann, A. and Jansen, E., 2019. Sea ice variability in the southern Norwegian Sea during glacial Dansgaard-Oeschger climate cycles. *Science advances*, *5*(3), p.eaau6174.

Samartin, S., Heiri, O., Lotter, A.F. and Tinner, W., 2012. Climate warming and vegetation response after Heinrich event 1 (16 700–16 000 cal yr BP) in Europe south of the Alps. *Climate of the Past*, *8*(6), pp.1913-1927.

Schillereff, D.N., Chiverrell, R.C., Macdonald, N. and Hooke, J.M., 2015. Flood stratigraphies in lake sediments: A review. *Earth-Science Reviews*, *135*, pp.17-37.

Shakun, J.D., Clark, P.U., He, F., Marcott, S.A., Mix, A.C., Liu, Z., Otto-Bliesner, B., Schmittner, A. and Bard, E., 2012. Global warming preceded by increasing carbon dioxide concentrations during the last deglaciation. *Nature*, 484(7392), p.49.

Sheldrick, C.D., 1997. *Plant macrofossil records from UK lake sediments spanning the last glacial-interglacial transition, ca. 14-9 C Ka BP. Unpublished PhD thesis,* University of London.

Smith, A.J.E. and Smith, R., 2004. *The moss flora of Britain and Ireland*. Cambridge University Press.

Soulié-Märsche, I. and Garcia, A., 2015. Gyrogonites and oospores, complementary viewpoints to improve the study of the charophytes (Charales). *Aquatic Botany*, 120, 7–17

Spence, D.H.N. and Chrystal, J., 1970. Photosynthesis and zonation of freshwater macrophytes. 1. Depth distribution and shade tolerance. *New phytologist*, *69*(1), 205-215.

Steffensen, J.P., Andersen, K.K., Bigler, M., Clausen, H.B., Dahl-Jensen, D., Fischer, H., Goto-Azuma, K., Hansson, M., Johnsen, S.J., Jouzel, J. and Masson-Delmotte, V., 2008. High-resolution Greenland ice core data show abrupt climate change happens in few years. *Science*, *321*(5889), pp.680-684.

Talbot, M.R., 1990. A review of the palaeohydrological interpretation of carbon and oxygen isotopic ratios in primary lacustrine carbonates. *Chemical Geology: Isotope Geoscience Section*, *80*(4), pp.261-279.

Taylor, B., 2011. Early Mesolithic activity in the wetlands of the Lake Flixton Basin. *Journal of Wetland Archaeology*, *11*(1), 63-84.

Treese, K.L. and Wilkinson, B.H., 1982. Peat-marl deposition in a Holocene paludal-lacustrine basin—Sucker Lake, Michigan. *Sedimentology*, *29*(3), 375-390.

1189 Tweddle, J.C., 2001. Regional vegetational history. In: Bateman, M.D., Buckland, P.C., Frederick, C.D.,
1190 Whitehouse, N.J. (Eds.), The Quaternary of East Yorkshire and North Lincolnshire Field Guide. Quaternary
1191 Research Association, London, pp. 35–46.

1192 Turney, C.S., Coope, G.R., Harkness, D.D., Lowe, J.J. and Walker, M.J., 2000. Implications for the dating of
1193 Wisconsinan (Weichselian) Late-Glacial events of systematic radiocarbon age differences between terrestrial
1194 plant macrofossils from a site in SW Ireland. *Quaternary Research*, 53(1), pp.114-121.

1195 Tye, G.J., Sherriff, J., Candy, I., Coxon, P., Palmer, A., McClymont, E.L. and Schreve, D.C., 2016. The $\delta^{18}O$
1196 stratigraphy of the Hoxnian lacustrine sequence at Marks Tey, Essex, UK: implications for the climatic structure
1197 of MIS 11 in Britain. *Journal of Quaternary Science*, *31*(2), pp.75-92.

1198 van Asch, N., Lutz, A. F., Duijkers, M. C., Heiri, O., Brooks, S. J., and Hoek, W. Z. 2012. Rapid climate change
1199 during the Weichselian Lateglacial in Ireland: Chironomid-inferred summer temperatures from Fiddaun, Co.
1200 Galway. *Palaeogeography, Palaeoclimatology, Palaeoecology*, *315*, 1-11.

1201 Van Geel, B., Bohncke, S.J.P. and Dee, H., 1980. A palaeoecological study of an upper Late Glacial and
1202 Holocene sequence from “De Borchert”, The Netherlands. *Review of Palaeobotany and Palynology*, *31*,
1203 pp.367-448.

1204 Van Geel, B., Coope, G. R., and Van Der Hammen, T. 1989. Palaeoecology and stratigraphy of the Lateglacial
1205 type section at Usselo (The Netherlands). *Review of Palaeobotany and Palynology*, *60*(1), 25-129.

1206 Vandenberghe, J., 2008. The fluvial cycle at cold–warm–cold transitions in lowland regions: a refinement of
1207 theory. *Geomorphology*, *98*(3-4), pp.275-284.

1208 Vellinga, M. and Wood, R.A., 2002. Global climatic impacts of a collapse of the Atlantic thermohaline
1209 circulation. *Climatic change*, *54*(3), pp.251-267.

1210 von Grafenstein, U., Erlenkeuser, H., Brauer, A., Jouzel, J. and Johnsen, S.J., 1999. A mid-European decadal
1211 isotope-climate record from 15,500 to 5000 years BP. *Science*, *284*(5420), 1654-1657.

1212 von Grafenstein, U., Eicher, U., Erlenkeuser, H., Ruch, P., Schwander, J. and Ammann, B., 2000. Isotope
1213 signature of the Younger Dryas and two minor oscillations at Gerzensee (Switzerland): palaeoclimatic and
1214 palaeolimnologic interpretation based on bulk and biogenic carbonates. *Palaeogeography, Palaeoclimatology,*
1215 *Palaeoecology*, *159*(3-4), 215-229.

1216 Wagner-Cremer, F. and Lotter, A.F., 2011. Spring-season changes during the Late Pleniglacial and
1217 Bølling/Allerød interstadial. *Quaternary Science Reviews*, *30*(15-16), 1825-1828.

1218 Walker, M.J.C., 1995. Climatic changes in Europe during the last glacial/interglacial transition. *Quaternary*
1219 *International*, *28*, pp.63-76.

1220 Walker, M.J.C., Coope, G.R. and Lowe, J.J., 1993. The Devensian (Weichselian) Lateglacial
1221 palaeoenvironmental record from Gransmoor, East Yorkshire, England: A contribution to the ‘North Atlantic
1222 seaboard programme’of IGCP-253,‘Termination of the Pleistocene’. *Quaternary Science Reviews*, *12*(8), 659-
1223 680.

1224 Walker, M.J.C., Coope, G.R., Sheldrick, C., Turney, C.S.M., Lowe, J.J., Blockley, S.P.E. and Harkness, D.D.,
1225 2003. Devensian Lateglacial environmental changes in Britain: a multi-proxy environmental record from
1226 Llanilid, South Wales, UK. *Quaternary Science Reviews*, *22*(5), 475-520.

1227 Watson, J.E., Brooks, S.J., Whitehouse, N.J., Reimer, P.J., Birks, H.J.B. and Turney, C., 2010. Chironomid-
1228 inferred late-glacial summer air temperatures from Lough Nadourcan, Co. Donegal, Ireland. *Journal of*
1229 *Quaternary Science*, *25*(8), 1200-1210.

1230 Watson, E.V., 1981. *British Mosses and Liverworts: An Introductory Work*. Cambridge University Press.

1231 Wohlfarth, B., Muschitiello, F., L. Greenwood, S., Andersson, A., Kylander, M., Smittenberg, R.H.,
1232 Steinthorsdottir, M., Watson, J. and Whitehouse, N.J., 2017. Hässeldala–a key site for Last Termination
1233 climate events in northern Europe. *Boreas*, *46*(2), pp.143-161.

1234 Wohlfarth, B., Luoto, T.P., Muschitiello, F., Väliranta, M., Björck, S., Davies, S.M., Kylander, M., Ljung, K.,
1235 Reimer, P.J. and Smittenberg, R.H., 2018. Climate and environment in southwest Sweden 15.5–11.3 cal. ka
1236 BP. *Boreas*, *47*(3), pp.687-710.

1237 Yu, Z. and Eicher, U., 1998. Abrupt climate oscillations during the last deglaciation in central North America.
1238 *Science*, *282*(5397), pp.2235-2238.

1239 Zhao, Y., Sayer, C.D., Birks, H.H., Hughes, M. and Peglar, S.M., 2006. Spatial representation of aquatic
1240 vegetation by macrofossils and pollen in a small and shallow lake. *Journal of Paleolimnology*, *35*(2), pp.335-
1241 350.